IEEE Access
Multidisciplinary | Rapid Review | Open Access Journal

Received April 21, 2017, accepted May 26, 2017, date of publication June 6, 2017, date of current version June 27, 2017.

Digital Object Identifier 10.1109/ACCESS.2017.2712359

Discrete Multi-Tone Digital Subscriber Loop Performance in the Face of Impulsive Noise

TONG BAI[1], (Student Member, IEEE), HONGMING ZHANG[1], (Student Member, IEEE), RONG ZHANG[1], (Senior Member, IEEE), LIE-LIANG YANG[1], (Fellow, IEEE), ANAS F. AL RAWI[2], (Member, IEEE), JIANKANG ZHANG[1], (Member, IEEE), AND LAJOS HANZO[1], (Fellow, IEEE)

[1]School of Eletronics and Computer Science, University of Southampton, Southampton, SO17 1BJ, U.K.
[2]Research and Technology, British Telecom, Adastral Park, Martlesham Heath, IP5 3RE, U.K.

Corresponding author: Lajos Hanzo (lh@ecs.soton.ac.uk)

This work was supported in part by the EPSRC projects under Grant EP/N004558/1 and Grant EP/N023862/1, in part by the European Research Councils Advanced Fellow Grant under the Beam-Me-Up Project, in part by the Royal Society's Wolfson Research Merit Award, and in part by the RAEng Industrial Fellow Grant. The data from the paper can be obtained from the University of Southampton ePrints research repository, https://doi.org/10.5258/SOTON/D0106.

ABSTRACT As an important solution to ''the last mile'' access, digital subscriber loops (DSLs) are still maintained in a huge plant to support low-cost but high-quality broadband network access through telephone lines. The discrete multi-tone (DMT) transmissions constitute a baseband version of the ubiquitous orthogonal frequency division multiplexing. While the DMT is ideally suited to deal with the frequency selective channel in DSL, the presence of bursty impulsive noise tends to severely degrade the transmission performance. In this paper, we analyze the statistics of impulsive noise and its effects on the received signals, with the aid of a hidden semi-Markov process. The closed-form bit error rate expression is derived for the DMT system for Q-ary quadrature amplitude modulation under practical noise conditions and for measured dispersive DSL channels. Instead of relying on the simplified stationary and impulsive noise process, our noise model considers both the temporal and spectral characteristics based on the measurement results. The simulation results confirm the accuracy of the formulas derived and quantify the impact both of the impulsive noise and of the dispersive channel in DSL.

INDEX TERMS Digital subscriber loops, discrete multi-tone, impulsive noise, dispersive channel, performance analysis.

NOMENCLATURE

$(\cdot)^T$ and $(\cdot)^*$	the transpose and the conjugate, respectively
$(\cdot)^H$ and $(\cdot)^{-1}$	the conjugate transpose and the inverse, respectively
$\mathcal{E}[\cdot]$	the expectation operator
$\mathcal{F}[\cdot]$	the continuous Fourier transform operator
$\boldsymbol{x}(l)$	lth element of $\boldsymbol{x}$
$\boldsymbol{\mathcal{F}}$	the normalized DFT matrix
$\boldsymbol{I}_N$	the $(N \times N)$-element identity matrix

GLOSSARY

2B1Q	Two-Binary One-Quaternary
ACF	Auto-Correlation Function
ADSL	Asymmetric DSL
ARQ	Automatic Repeat reQuest
AWGN	Addictive White Gaussian Noise
BER	Bit Error Rate
BT	British Telecom
CAP	Carrierless Amplitude Modulation/Phase Modulation
CDF	Cumulative Density Function
CO	Central Offices
CP	Customer Premises
DFT	Discrete Fourier Transform
DMT	Discrete Multitone
DSL	Digital Subscriber Lines
DSLAM	DSL Access Multiplexer
DSM	Dynamic Spectrum Management
DT	Deutsche Telekom
ECM	Expanded Constellation Mapping
FTTdp	fibre-to-the-distribution-point

FTTH	fibre-to-the-home
HDSL	High-rate DSL
HSMM	Hidden Semi-Markov Model
IDFT	Inverse Discrete Fourier Transform
ISDN	Integrated Services Digital Network
ISI	Inter-Symbol Interference
LDPC	Low Density Parity-Check Codes
LUT	Look-up Table
MRP	Markov Renewable Process
OFDM	Orthogonal Frequency Division Multiplexing
PAM	Phase Amplitude Modulation
PDF	Probability Density Function
QAM	Quadrature Amplitude Modulation
RS	Reed-Solomon Codes
SCM	Single Carrier Modulation
SNR	Signal-to-Noise Ratio
SSM	Static Spectrum Management
TCM	Trellis Coded Modulation
THP	Tomlinson-Harashima Precoding
VDSL	Very-high-speed DSL
ZFP	Zero-Forcing Precoding

I. INTRODUCTION

The popularity of the wired broadband network is pushing them towards their limits. The fibre-to-the-home (FTTH) concept, which is expected to satisfy the escalating throughput demands, is still not a ubiquitous reality at the time of writing, since its installation is costly and in historic architectural regions it is outright banned. Hence the fibre-to-the-distribution-point (FTTdp) architecture relies on ''the last mile'' copper twisted pairs, but supports high-quality broadband network access. The G.fast Digital Subscriber Loops (DSL) [1]–[4], is capable of supporting a data rate of upto 1Gbps over copper twisted pairs.

The branching induces impairments in the existing DSL and imposes reflection points, resulting in dispersive propagation. Measurement results show that the coherence bandwidth of the channel is rather limited and hence the signal is transmitted over a channel exhibiting a frequency-selective transfer function, which causes inter-symbol interference (ISI). In order to mitigate the ISI, DSL transceivers employ the discrete multi-tone (DMT) technique, which is a baseband version of the orthogonal frequency division multiplexing (OFDM) [5].

Upon increasing the transmission rate over copper twisted pairs, they become increasingly prone both to the crosstalk and to the impulsive noise. The crosstalk can be substantially mitigated by the duplex transmission techniques of [6] and by the dynamic spectrum management of [7] and [8] as well as by the vectored transmission of [9] and [10]. However, the DMT block duration of the VDSL [11] is reduced from 125 μs to 20.83 μs in the recent G.fast standard [3], which increases the system's vulnerability to impulsive noise, because the impulsive noise is more likely to obliterate an entire DMT symbol instead of a small fraction of a single DMT symbol. If only a small fraction of a DMT symbol is wiped out, it can still be corrected by powerful channel coding. By contrast, if a whole DMT symbol is contaminated by the impulsive noise, the transmission reliability is severely degraded, because the forward error correction coding is overloaded and hence violently precipitates errors. Against the background, the performance of the DMT system suffering both from dispersion and from impulsive noise in DSL is analysed in this paper.

The impulsive noise in DSL can be categorized into internally and externally induced classes [12]. Externally induced impulses are inflicted by high-voltage devices, railways, fluorescent tubes, lightning, etc. whereas the internal ones are caused by dialling pulses, busy signals, ringing, etc. In the literature, two special cases of the popular multi-component Gaussian mixture model [13] have been used, namely the Bernoulli-Gaussian model [14] and the Middleton Class-A model [15]. However, these impulsive noise samples of these models are usually generated discontinuously, which fails to reflect the bursty nature of the impulsive noise in DSL.

The practical impulsive noise in DSL can be modelled by the following four characteristics: voltage amplitude, duration, inter-arrival time (the time between the arrival of two impulses) and the auto-correlation function. The first practical modelling of impulsive noise in twisted copper pairs dates back to as early as 1962 [16]. Fano's paper [17] characterized the complementary distribution of the inter-arrival time of the impulses obeying the product of the Pareto distribution and of the exponential distribution. Henkel *et al*. [12], [18] characterised the impulsive noise of DSL both in the time domain and the frequency domain based on the measurement results of Deutsche Telekom (DT) carried out for asymmetric DSL (ADSL). Levey and McLaughlin [19] modelled the inter-arrival time using a Markov renewal process (MRP), where the states obeyed the above-mentioned product of Pareto and exponential distributed variables. Mann *et al*. [20] modelled the voltage amplitude by the classic Weibull distribution and proposed an improved technique of generating the impulsive noise exhibiting a more realistic spectral variability based on the measurement results both of DT and of British Telecom (BT). Over the years the models have become more realistic, step-by-step.

The research of Ghosh has analysed the effect of the impulsive noise on quadrature amplitude modulation (QAM) [14] with the aid of a Bernoulli-Gaussian noise model, albeit the model fails to reflect the bursty characteristics of the impulsive noise in DSL. Based on the noise model of Henkel and Keßler [12], the performance of a binary single carrier system in the local loop has been examined by Chew *et al*. [21]. However, the single carrier modulation has been replaced by the DMT in the recent DSL standards. This is because every time the signalling rate of a single-carrier system is doubled, the length of the channel equalizer expressed in terms of the number of symbols transmitted also has to be doubled. By contrast, in DMT-transmissions a single-tap frequency-domain equalizer can be used. Based on the model by Mann *et al*. [20], the bit error rate (BER) of both PAM

as well as of the single carrier QAM and of multicarrier QAM was studied under the Bernoulli-Weibull model by Nedev *et al*. [22], where the accuracy of the simplified Bernoulli-Weibull model remained limited.

Against this background, we analyse the performance of discrete multi-tone systems in practical scenarios. Our main contributions are as follows:

1) we commence by a brief survey of the development of copper-based data-communications from a physical-layer perspective;
2) we conceive both a stationary and an impulsive noise model, which is capable of accurately reflecting both the temporal and spectral characteristics of practical channels;
3) to accurately model the non-Gaussian coloured impulsive noise in DSL, a look-up table (LUT) is necessary for characterising the relationship between the auto-correlation function of Gaussian distributed variables and the target Weibull distributed variables. We provide a computationally convenient expression for populating the LUT based on the memoryless nonlinear transform function proposed in [20];
4) with the aid of a Hidden Semi-Markov process, we derive the closed-form BER formula of DMT-based DSL systems relying on Q-ary QAM under a practical noise model and a dispersive channel;
5) we verify the accuracy of our BER formula by simulation results, where the dispersive channel is extended to 106 MHz, which is the bandwidth of the first version of G.fast.

The rest of the paper is organized as follows. We briefly introduce the historic development of DSL in Section II. Section III details the DMT system as well as the modelling and generation of the noise processes in DSL. In Section IV, we investigate the statistics of the noise samples both in the time domain and in the frequency domain. In Section V, we analyse the impact of the coloured non-Gaussian noise on the DMT/OFDM system and derive closed-form BER expressions. In Section VI, the BER performance of DMT-based DSL systems under practical noise conditions and measurement-based dispersive channel conditions is presented. Finally, the paper is concluded in Section VII.

II. HISTORICAL DEVELOPMENT OF DSL

Telephone lines date back to Alexander Graham Bell's invention of the telephone in 1875, when a single voice signal was transmitted within a 3.4kHz-bandwidth channel [6]. With the ever-increasing demand for data service since the 1970s, the feasibility of the twisted copper pair to convey data has drawn a huge amount of attention. DSL technologies enable high-speed digital transmission over the conventional telephone line.

Fig. 1 presents the achievable rate of the generations of DSL. The initial modem was not designed for supporting simultaneous telephone services and data services. This problem was solved by the integrated services digital

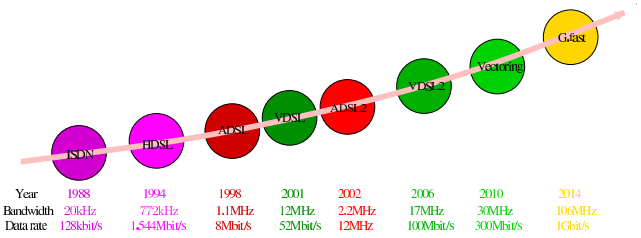

FIGURE 1. Illustration of the evolution of DSL.

network (ISDN). Designed for short range data services, the high-rate digital subscriber line (HDSL) was capable of supporting data traffic amongst buildings within a campus network. Asymmetric DSL (ADSL) was developed to support asymmetric data transmission by sharing the bandwidth between downstream and upstream. With data rate of upto 8Mbit/s for the downstream, the true broadband era has arrived at the end of the 20th century. ADSL2 improved the peak downstream rate to 12Mbit/s by extending the bandwidth from 1.1MHz to 2.2MHz and by introducing the digital subscriber line access multiplexer (DSLAM), which is deployed near the customer premises. Very high-speed DSL (VDSL) extended the bandwidth further, upto 17MHz and 30MHz for the most recent edition termed as VDSL2. However, with the increase of the operating frequencies, crosstalk among copper pairs becomes a challenge. Hence the so-called vectoring techniques were designed for reducing the influence of crosstalk, hence boosting the data rate upto 100Mbit/s. At the time of writing, experts from industry and academia are working on a new standard for DSL, namely G.fast, which is capable of providing 500Mbit/s to 1000Mbit/s over copper wires within a distance of 100 meters for fibre-to-the-building deployment. During the evolution of DSL, increasing number of both advanced communication and signal processing techniques have been gradually adopted. In the following part of the section, we will briefly review them with the reference to Fig. 2, which plots DSL techniques categorized by various physical-layer aspects.

A. MODULATION

The binary information bits are mapped to the symbols of either DMT or of single-carrier modulation (SCM) known as two-binary one-quaternary (2B1Q), carrierless AM/PM (CAP) and quadrature amplitude modulation (QAM). Sugimoto *et al*. designed the transceiver of 2B1Q for ISDN [23], which relies on a four-level pulse amplitude modulation (PAM). Im and Werner proposed a crosstalk equalization technique for the CAP [24], which is a two-dimensional passband transmission scheme. Daneshrad and Samueli analysed the performance of QAM in DSL [25], which is based on baseband spectral shaping techniques, while Chow *et al*. proposed the classic DMT [26]. Shim and Shanbhag compared the complexity of the above single-carrier and multicarrier modulation schemes in the high-rate VDSL scenario [27].

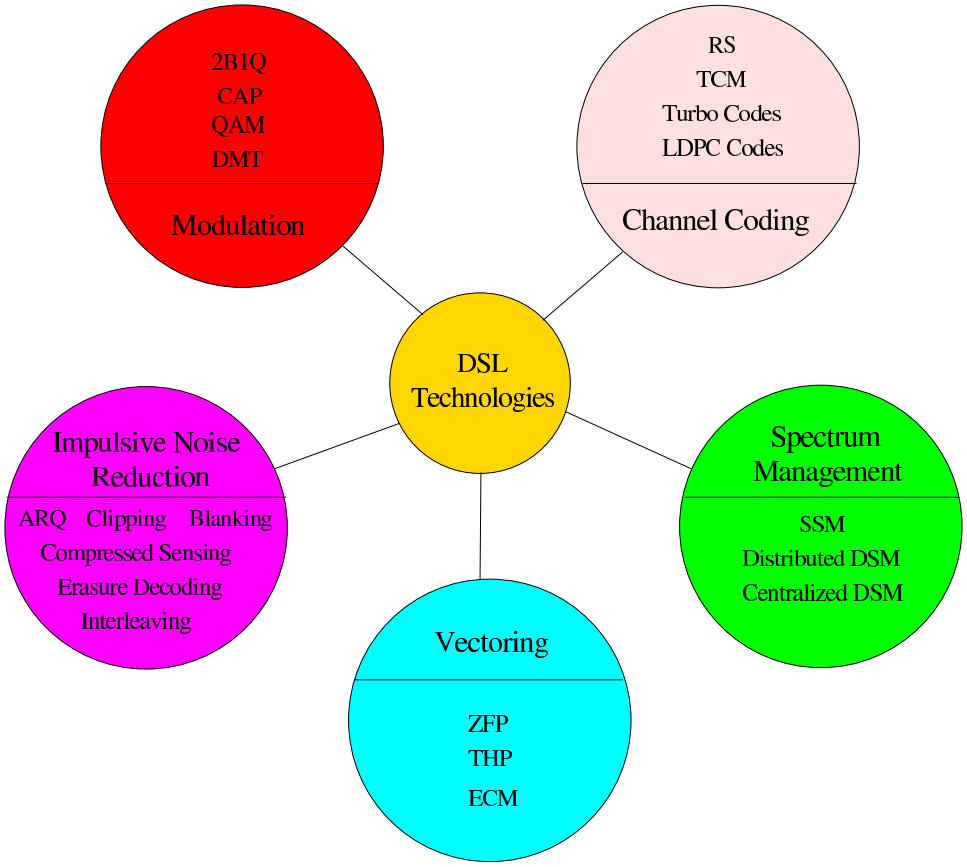

FIGURE 2. Illustration of DSL techniques from a physical-layer perspective. The abbreviations are defined as follows: two-binary one-quaternary (2B1Q), carrierless AM/PM (CAP), quadrature amplitude modulation (QAM). discrete multitone (DMT), Reed-Solomon codes (RS), trellis coded modulation (TCM), low density parity-check (LDPC), automatic repeat request (ARQ), zero-forcing precoding (ZFP), Tomlinson-Harashima precoding (THP) and expanded constellation mapping (ECM), static spectrum management (SSM), dynamic spectrum management (DSM).

B. CHANNEL CODING

The low-power received signals are susceptible both to impulsive noise and to crosstalk, but fortunately the attainable system performance can be improved by using forward error correction (FEC) codes. Reed-Solomon (RS) codes and trellis coded modulation (TCM) have been incorporated into ADSL and VDSL, but at the time of writing the intention is to replace them by more powerful codes, such as turbo codes [28] or low density parity-check (LDPC) codes [29]. Kerpez examined the performance of RS codes in ADSL [30] in the presence of impulsive noise. Later Kerpez and Sistanizadeh investigated the performance of TCM in DSL [31]. Eleftheriou *et al*. discussed both the performance and latency as well as complexity both of turbo codes and of LDPC codes in DSL [32].

C. IMPULSIVE NOISE REDUCTION

As discussed in Section I, impulsive noise has been a challenging problem in DSL, which has drawn substantial attention [33]–[39]. Considering that the impulsive noise does not occur frequently, Neckebroek *et al*. proposed retransmission schemes in [33] for DSL. Interleaving [34] is another low-complexity technique of reducing the effects of impulsive noise, albeit at the cost of increasing the delay. Toumpakaris and Cioffi designed erasure decoding aided RS decoding [35] for reducing the interleaving delay. To mitigate the effect of impulsive noise, Zhidkov conceived various low-complexity schemes, such as clipping and blanking, for a general OFDM scenario [36]. Quite recently, compressed sensing has also been proposed for impulse-noise mitigation [38], [39].

D. VECTORING

With the increase of the operating frequencies, both the attenuation of the channel and the power of far-end crosstalk (FEXT) becomes higher. Since the transmitters are co-located for the downstream transmission, transmit precoding (TPC) can be applied to the transmitted signal so that it arrives at customers without crosstalk [10]. Cendrillon *et al*. proposed linear zero-forcing precoding (ZFP) and demonstrated that it was near-optimal under the scenario of low operating frequencies in DSL [40].

Ginis and Cioffi introduced the concept of Tomlinson-Harashima precoding (THP) [41] into DSL [9], which has a better performance than ZFP. Recently, Zhang *et al*. proposed a vector perturbation [42], [43] based method, namely the expanded constellation mapping (ECM) [44], which achieved a near-capacity performance.

E. SPECTRUM MANAGEMENT

Power control is one of the most pivotal issues in the interference-limited multiuser DSL system, where each user's rate is dependent both on its own power allocation and on that of others', because the signals from others impose crosstalk in DSL, especially at the high frequencies, which causes a degradation of the sum rate [8]. In order to make use of the high frequencies, efficient spectrum management techniques must be employed. The very basic method is static spectrum management (SSM), which allocates an identical power to each user [45]. By contrast, dynamic spectrum management (DSM) adaptively allocates a frequency-dependent power to the different users. Yu *et al*. proposed one of the first distributed DSM algorithms using iterative water-filling [7], which operates entirely autonomously. Xu *et al*. designed a low-complexity centralized DSM algorithm [46] for DSL, which is capable of finding the globally optimal solution, but requires a central hub supplied with full knowledge of the network's status.

III. SYSTEM AND NOISE MODELLING

A. DMT SIGNALLING

Again, the multipath channel severely degrades the performance of DSL systems. The transmitted signal after inverse discrete Fourier transform (IDFT) based modulation becomes real-valued [26]. The transmission bandwidth is divided into a number of subchannels having a bandwidth lower than the coherence bandwidth of the channel, which ensures that the signals of each substream experience flat fading.

In DMT systems, $(N-2)/2$ Q-ary QAM symbols are used to form a block of symbols $\boldsymbol{X} = [X_0, X_1, \cdots, X_{N-1}]^{\mathrm{T}}$ having a Hermitian transpose structure, implying that we have $X_n = X^*_{N-n}$ and $X_0 = X_{N/2} = 0$. The block of symbols is serial-to-parallel converted and the resultant parallel symbols are transformed to the time-domain with the aid of IDFT, resulting in the real-valued time-domain signals of $\boldsymbol{x} = [x_0, x_1, \cdots, x_{N-1}]^{\mathrm{T}}$, which can be expressed as

$$\boldsymbol{x} = \boldsymbol{\mathcal{F}}^H \boldsymbol{X}, \tag{1}$$

where $\boldsymbol{\mathcal{F}}$ is the normalized discrete Fourier transform (DFT) matrix [47], yielding $\boldsymbol{\mathcal{F}}\boldsymbol{\mathcal{F}}^H = \boldsymbol{\mathcal{F}}^H\boldsymbol{\mathcal{F}} = \boldsymbol{I}_N$, which means that $\boldsymbol{\mathcal{F}}$ is an orthogonal matrix.

In order to avoid ISI, cyclic prefices are added to the parallel-to-serial converted symbols, resulting in

$$\tilde{\boldsymbol{x}} = [x_{N-\mu}, x_{N-\mu+1}, \cdots, x_{N-1}, x_0, x_1, \cdots, x_{N-1}]^{\mathrm{T}}, \tag{2}$$

where μ is the length of the cyclic prefices, which should be selected by obeying the constraint of

$$\mu \Delta t \geq \tau_{max}, \tag{3}$$

where Δt is the sampling period at the baseband and τ_{max} is the maximum delay spread of the channel.

The time-domain signals $\tilde{\boldsymbol{x}}$ are passed through the dispersive DSL channel and are contaminated by the noise

$$\tilde{\boldsymbol{y}} = \boldsymbol{h}\tilde{\boldsymbol{x}} + \boldsymbol{u_S} + \boldsymbol{u_I}, \tag{4}$$

where $\tilde{\boldsymbol{y}}$ is a $(N+\mu)$-element vector, $\boldsymbol{h}$ is $(N+\mu)\times(N+\mu)$-element matrix, while the stationary noise $\boldsymbol{u_S}$ and the impulsive noise $\boldsymbol{u_I}$ are $(N+\mu)$-element vectors.

The cyclic prefices received are discarded, because they are contaminated by the ISI and (4) becomes equivalent to

$$\boldsymbol{y} = \tilde{\boldsymbol{h}}\boldsymbol{x} + \tilde{\boldsymbol{u}}_{\boldsymbol{S}} + \tilde{\boldsymbol{u}}_{\boldsymbol{I}}, \tag{5}$$

where $\boldsymbol{y}$ is an N-element vector, $\tilde{\boldsymbol{h}}$ is an $(N \times N)$-element matrix, while $\tilde{\boldsymbol{u}}_{\boldsymbol{S}}$ and $\tilde{\boldsymbol{u}}_{\boldsymbol{I}}$ are N-element vectors.

Assuming that synchronization is perfectly achieved at the receiver, the received symbols can be recovered with the aid of a DFT based demodulator as:

$$\begin{aligned}\boldsymbol{Y} &= \boldsymbol{\mathcal{F}}\boldsymbol{y} = \boldsymbol{\mathcal{F}}(\tilde{\boldsymbol{h}}\boldsymbol{x} + \tilde{\boldsymbol{u}}_{\boldsymbol{S}} + \tilde{\boldsymbol{u}}_{\boldsymbol{I}}) \\ &= \boldsymbol{\mathcal{F}}(\tilde{\boldsymbol{h}}\boldsymbol{\mathcal{F}}^H\boldsymbol{X} + \tilde{\boldsymbol{u}}_{\mathrm{S}} + \tilde{\boldsymbol{u}}_{\boldsymbol{I}}) \\ &= \boldsymbol{\mathcal{F}}\boldsymbol{\mathcal{F}}^H\boldsymbol{H}\boldsymbol{\mathcal{F}}\boldsymbol{\mathcal{F}}^H\boldsymbol{X} + \boldsymbol{\mathcal{F}}\tilde{\boldsymbol{u}}_{\boldsymbol{S}} + \boldsymbol{\mathcal{F}}\tilde{\boldsymbol{u}}_{\boldsymbol{I}} \\ &= \boldsymbol{H}\boldsymbol{X} + \boldsymbol{U_S} + \boldsymbol{U_I}, \end{aligned} \tag{6}$$

where $\tilde{\boldsymbol{h}}$ can be diagonalized by the DFT matrix, giving $\tilde{\boldsymbol{h}} = \boldsymbol{\mathcal{F}}^H\boldsymbol{H}\boldsymbol{\mathcal{F}}$. The received symbols having an index spanning from 1 to $(\frac{N-2}{2})$ are used for detection. Since the DSL channel is only slowly time-variant [6], it is reasonable to assume perfect channel estimation. Hence $\boldsymbol{H}$ can be equalized by a one-tap frequency-domain channel equalizer (FEQ) at the receiver. $\boldsymbol{U}_{\mathrm{S}} = \boldsymbol{\mathcal{F}}\tilde{\boldsymbol{u}}_{\mathrm{S}}$ is the DFT of $\tilde{\boldsymbol{n}}_{\mathrm{S}}$, which is also an AWGN process since $\boldsymbol{\mathcal{F}}$ is unitary. $\boldsymbol{U_I} = \boldsymbol{\mathcal{F}}\tilde{\boldsymbol{u}}_{\boldsymbol{I}}$ is the DFT of $\tilde{\boldsymbol{u}}_{\boldsymbol{I}}$ and represents the impulsive noise in the frequency domain.

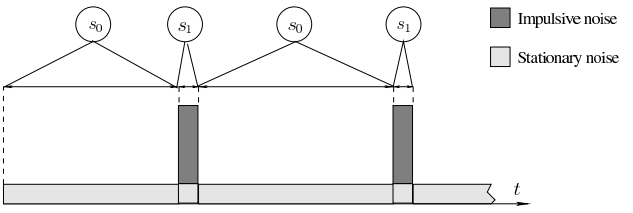

FIGURE 3. Illustration of noise process model, s_0 meaning states without impulsive noise and s_1 meaning states with impulsive noise.

B. NOISE PROCEDURE MODELLING

The noise in DSL can be categorized into stationary noise and impulsive noise, which can be modelled by a Hidden Semi-Markov Model (HSMM) [49]–[51], where the different states may have different durations and distributions. As shown in Fig 3, the noise in the time domain is represented by two states, where state s_0 refers to the absence of the impulsive noise, while state s_1 refers to the presence of both the stationary noise and the impulsive noise. It is reasonable to assume that the noise process starts from each state with an identical probability of 0.5.

Below both the stationary and impulsive noise are characterized by their amplitude as well as temporal and spectral statistics.

1) STATIONARY NOISE

As illustrated in [18], the power spectrum of stationary noise is flat over all frequencies and the amplitude is Gaussian distributed. The probability density function (PDF) of the stationary noise is expressed as

$$f(u_S) = \frac{1}{\sqrt{2\pi}\sigma_S} \exp\left(-\frac{|u_S|^2}{2\sigma_S^2}\right), \tag{7}$$

where u_S is real and σ_S^2 denotes the stationary noise variance.

2) AMPLITUDE OF THE IMPULSIVE NOISE

Based on the results of [20], the amplitude of the impulse noise can be modelled by the Weibull distribution of

$$f(u_I) = \frac{1}{2}ab|u_I|^{a-1} \exp\left(-b|u_I|^a\right), \tag{8}$$

where u_I is real while a and b characterize the amplitude in different environments and locations.

3) DURATION OF THE IMPULSIVE NOISE

As the measurement results of [20] illustrated, the duration of the impulse noise may be characterized by a two-term log-normal form. The probability density function (PDF) of the duration can be expressed as

$$f(t|s_1)) = B\frac{1}{\sqrt{2\pi}v_1 t} \exp\left(-\frac{\ln^2(t/t_1)}{2v_1^2}\right) + (1-B)\frac{1}{\sqrt{2\pi}v_2 t} \exp\left(-\frac{\ln^2(t/t_2)}{2v_2^2}\right). \tag{9}$$

The typical parameter values for several practical environments, such as customer premises and central offices measured by DT, by BT and by the Italian Public Switched Telephone Network (PSTN) are summarized in Table 1.

TABLE 1. Parameter values for characterising impulsive noise amplitude and duration [20], [37].

	a	b	B	v_1	t_1	v_2	t_2
BT(CP)	0.263	4.77	0.45	1.25	1.3 μs	21.5	129 μs
DT(CP)	0.486	44.40	1	1.15	18 μs	\	\
DT(CO)	0.216	12.47	0.25	0.75	8 μs	1.0	125 μs
PSTN	0.98	100	0.7	0.53	4.5 μs	0.8	60 μs

4) INTER-ARRIVAL TIME OF THE IMPULSIVE NOISE

Setting the ranges of inter-arrival times as Markov states, as suggested in [20], the two-state MRP model is capable of characterising the impulsive noise inter-arrival times in DSL systems. To elaborate, $s_{0,0}$ represents the inter-arrival times lower than 1 ms, which is exponentially-distributed; $s_{0,1}$ represents the inter-arrival time longer than 1 ms, which is Pareto-distributed. Since only the inter-arrival time shorter than 1 ms obeys the exponential distribution, the PDF of state s_0 should be reformatted as a truncated distribution. Therefore, the PDF of the two states of the inter-arrival time can be expressed as

$$f(t|s_{0,j}) = \begin{cases} \dfrac{1}{1-\exp(-\lambda t_s)}\lambda \exp(-\lambda t), & \text{if } j = 0 (t < t_s) \\ \theta t_s^{\theta}/t^{\theta+1}, & \text{if } j = 1 (t \geq t_s), \end{cases} \tag{10}$$

where $t_s = 1$ ms, which is the switching threshold of the two states, while we have $\lambda = 0.16s^{-1}$ and $\theta = 1.5$ [20].

The Markov state-transition probability matrix of state s_0 is a (2×2) - element matrix

$$\mathbf{P}_{s_0}(1) = \begin{bmatrix} p_{s_0}^{00} & p_{s_0}^{01} \\ p_{s_0}^{10} & p_{s_0}^{11} \end{bmatrix}, \tag{11}$$

and the typical state transition probabilities are shown below, which were confirmed by χ^2-type hypothesis testing in [20] based on the experimental measurement results, yielding:

$$\mathbf{P}_{s_0}(1) = \begin{bmatrix} 0.8 & 0.2 \\ 0.4 & 0.6 \end{bmatrix}. \tag{12}$$

5) SPECTRAL CHARACTERISTICS OF NOISE

In order to generate the noise process having statistically accurate characteristics both in the time- and in the frequency-domain, the stationary noise has a white spectrum while the normalized auto-correlation function (ACF) of the impulsive noise is modelled by the exponentially decaying cosine function of [20]

$$R(t) = cos(2\pi\alpha t) \exp\left(-\beta|t|\right), \tag{13}$$

where α is randomly generated by obeying the Gaussian distribution, while β is a randomly generated Gaussian variable related to the duration of impulsive noise spikes [51].

C. IMPULSIVE NOISE GENERATION

It can be inferred from the above discussions that the impulsive noise is a correlated non-Gaussian signal. The generation of a random sequence having a jointly specified marginal distribution and auto-correlation has attracted substantial research attention [52]–[54]. One of the most popular methods is the so-called zero memory non-linearity (ZMNL) technique [52], which transforms a zero-mean unit-variance Gaussian sequence associated with the corresponding ACF to another sequence having a specific target cumulative density function (CDF) and target ACF.

Since our signals are processed at discrete time instants, we denote the discrete time index by d. The generation of the impulsive noise process is detailed step-by-step in Fig 4:

1) Generate a white Gaussian sequence $\hat{\boldsymbol{n}}_{\boldsymbol{L}}$ obeying $\mathcal{N}(0, 1)$ with the duration L, which is randomly generated according to the duration PDF of every impulse state;

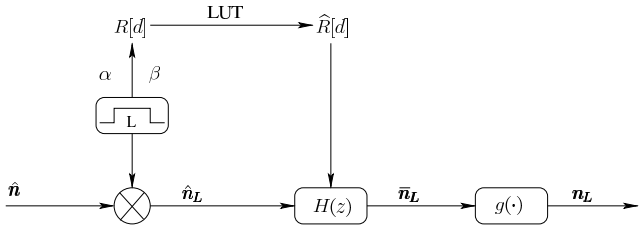

FIGURE 4. Illustration of the impulsive noise generation scheme.

2) Obtain the discrete target ACF $R[d]$ by calculating the IDFT of $\sigma_{I,i}$ in (32) with α and β adjusted according to the their distribution and to the above impulsive noise duration L;
3) Obtain the corresponding discrete ACF $\hat{R}[d]$ for the Gaussian sequences by matching $R[d]$ to the look-up table (LUT), which is detailed later in this section;
4) Design a filter $H(z)$ with the aid of the Levinson algorithm of [55] to generate the output signal obeying the ACF of $\hat{R}[d]$;
5) Pass the white Gaussian sequence $\hat{\boldsymbol{n}}_{\boldsymbol{L}}$ through the filter and normalize the variance of the output $\bar{\boldsymbol{n}}_{\boldsymbol{L}}$ to unity;
6) Pass the correlated Gaussian sequence $\bar{\boldsymbol{n}}_{\boldsymbol{L}}$ through the ZMNL function $g(\cdot)$ to get the target correlated Weibull distributed sequence $\boldsymbol{n}_{\boldsymbol{L}}$.

In the following, we will characterize the ZMNL function and the relationship between $R[d]$ and $\hat{R}[d]$. Let us denote the CDF of $\boldsymbol{n}_{\boldsymbol{L}}$ as F_{n_L} and CDF of $\bar{\boldsymbol{n}}_{\boldsymbol{L}}$ as $F_{\bar{n}_L}$. Then, we have

$$F_{n_L} = \int_{-\infty}^{n_L} f(u_I)\,\mathrm{d}u_I = \begin{cases} \frac{1}{2}\exp\left[-b(-n_L)^a\right], & n_L \le 0 \\ 1-\frac{1}{2}\exp\left[-b(n_L)^a\right], & n_L > 0. \end{cases} \tag{14}$$

Then, for the standard normal distribution, we have:

$$F_{\bar{n}_L} = \frac{1}{2}\left[1+\mathrm{erf}\left(\frac{\bar{n}_L}{\sqrt{2}}\right)\right]. \tag{15}$$

The ZMNL function is expressed as [52]

$$g(x) = F_{n_L}^{-1}\left[F_{\bar{n}_L}(x)\right] = \begin{cases} -\left[\frac{1}{b}\ln\left(\frac{1}{\mathrm{erfc}(-x/\sqrt{2})}\right)\right]^{\frac{1}{a}}, & x \le 0 \\ \left[\frac{1}{b}\ln\left(\frac{1}{\mathrm{erfc}(x/\sqrt{2})}\right)\right]^{\frac{1}{a}}, & x > 0. \end{cases} \tag{16}$$

In order to obtain the discrete target ACF $R[d]$, the corresponding discrete ACF $\hat{R}[d]$ has to be the solution of [52]

$$R[d] = \sum_{k=1}^{\infty} c_k^2 \left(\hat{R}[d]\right)^k, \tag{17}$$

where we have

$$c_k^2 = \frac{1}{k!}\left[\int_{-\infty}^{\infty} g(x)H_k(x)\phi(x)\,\mathrm{d}x\right]^2, \tag{18}$$

and $H_k(x)$ is the kth physicists' Hermite polynomial [56] and $\phi(x)$ is the unit-variance normal probability density function. In this way, a look-up table (LUT) can be generated, matching $R[d]$ to the corresponding $\hat{R}[d]$.

IV. STATISTICS OF NOISE SAMPLES

A. NOISE CHARACTERISTICS IN THE TIME DOMAIN

Assuming that perfect synchronization is achieved at the receiver, the received samples arrive at the time instant of $0, \Delta t, 2\Delta t, \cdots, (N-1)\Delta t$, where $\Delta t = T_{\mathrm{DMT}}/N$ and T_{DMT} is the duration of a DMT symbol. The normalized state-duration d, which corresponds to the number of samples during that state is defined as $d = [t/\Delta t]$, where $[x]$ represents the integer closest to x. For convenience, let us denote $\frac{p_{s_0}^{10}}{p_{s_0}^{01}+p_{s_0}^{10}}$ and $\frac{p_{s_0}^{01}}{p_{s_0}^{01}+p_{s_0}^{10}}$ in (11) by $\pi_{0,1}$ and $\pi_{0,0}$, respectively. According to Appendix A, the probability mass functions (PMFs) of d conditioned on state s_0 and s_1 can be expressed as

$$p(d|s_0) = \begin{cases} \dfrac{\pi_{0,0}\left(e^{-\lambda\Delta t(d-0.5)} - e^{-\lambda\Delta t(d+0.5)}\right)}{1-e^{-\lambda t_s}}, & \text{if } d < [\frac{t_s}{\Delta t}] \\ \pi_{0,1}\left(\frac{t_s}{\Delta t}\right)^{\theta}\left(\frac{1}{(d-0.5)^{\theta}} - \frac{1}{(d+0.5)^{\theta}}\right), & \text{if } d \ge [\frac{t_s}{\Delta t}], \end{cases} \tag{19}$$

$$p(d|s_1) = B\left[Q\left(\frac{\ln(\frac{(d-0.5)\Delta t}{t_1})}{v_1}\right) - Q\left(\frac{\ln(\frac{(d+0.5)\Delta t}{t_1})}{v_1}\right)\right] + (1-B)\left[Q\left(\frac{\ln(\frac{(d-0.5)\Delta t}{t_2})}{v_2}\right) - Q\left(\frac{\ln(\frac{(d+0.5)\Delta t}{t_2})}{v_2}\right)\right]. \tag{20}$$

B. NOISE CHARACTERISTICS IN THE FREQUENCY DOMAIN

The noise in the frequency domain can also be categorized by two states: S_0 represents the absence of impulsive noise in a DMT symbol and S_1 refers to the presence of impulsive noise in a DMT symbol. In contrast to the time-domain, where the state transitions occur at multiples of Δt, in the frequency-domain the state transitions occur at multiples of the DMT symbol duration, because the impulsive noise effects are spread over the entire DMT symbol, when the signal is transformed from the time-domain back to the frequency-domain.

As shown in Fig 5, we define the duration of a state in the frequency-domain as D, which is a multiple of the DMT symbol duration. For convenience, we define the number of samples before time-domain state transition in the DMT symbol by η, where the frequency-domain state transition occurs. Since η is the offset relative to the start instant of a DMT symbol, η can be readily assumed to obey the uniform

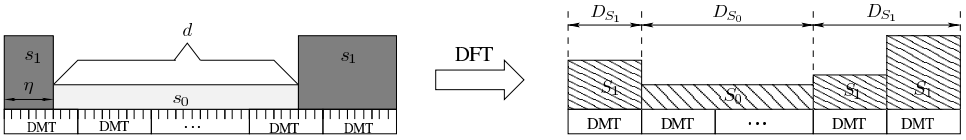

FIGURE 5. Illustration of the impulsive noise effect imposed DMT both in the time domain (left) and the frequency domain (right).

distribution of

$$p(\eta) = \frac{1}{N}, \quad \eta = 0, 1, \cdots, N-1. \tag{21}$$

Under the above assumptions, the relationship between the duration d of state s_i, where $i \in \{0, 1\}$ and the corresponding duration D of state S_i, where $i \in \{0, 1\}$, may be readily shown. For state s_0, we have

$$D = \begin{cases} \lceil d/N \rceil - 2, & \text{if } \eta + d < \lceil d/N \rceil N \ \& \ \eta \neq 0 \\ \lceil d/N \rceil - 1, & \text{if } \eta + d \geq \lceil d/N \rceil N \ \& \ \eta \neq 0 \\ & \text{or } \eta + d > \lceil d/N \rceil N \ \& \ \eta = 0 \\ \lceil d/N \rceil, & \text{if } \eta + d = \lceil d/N \rceil N \ \& \ \eta = 0, \end{cases} \tag{22}$$

while for state s_1, we have

$$D = \begin{cases} \lceil d/N \rceil, & \text{if } \eta + d \leq \lceil d/N \rceil N \\ \lceil d/N \rceil + 1, & \text{if } \eta + d > \lceil d/N \rceil N, \end{cases} \tag{23}$$

where $\lceil x \rceil$ denotes the smallest integer larger than x.

As shown in Appendix B, the PMF $p(D|S_0)$ and $p(D|S_1)$ of D conditioned on state S_0 and S_1 can be readily derived.

C. IMPULSIVE NOISE OCCURRENCE IN A DMT SYMBOL

Let us assume that the noise process matches the statistical distribution required for the noise model sufficiently accurately. Here, we denote the total number of the states S_i as K_i, where $i \in \{0, 1\}$, during the noise process. Since the two states occur alternatively, we have $K_0 = K_1$. As shown in Fig. 5, let us denote the duration of the kth state S_i as $D_{S_i,k}$ and the expectation of $\cdot$ by $\mathcal{E}[\cdot]$. Then, we have $\sum_{k=1}^{K_i} D_{S_i,k} \rightarrow \mathcal{E}[D_{S_i,k}]K_i$. Hence, the posteriori probability of an observed DMT symbol Y in (6), which is corrupted by the noise in the state S_i can be expressed as

$$P(S_i|\boldsymbol{Y}) = \frac{\mathcal{E}[D_{S_i,k}]}{\mathcal{E}[D_{S_0,k}] + \mathcal{E}[D_{S_1,k}]}. \tag{24}$$

According to Bayes's rule, we have

$$\begin{aligned} P(D, S_i|\boldsymbol{Y}) &= \frac{P(D, S_i, \boldsymbol{Y})}{P(\boldsymbol{Y})} \\ &= \frac{P(D|S_i, \boldsymbol{Y})P(S_i, \boldsymbol{Y})}{P(\boldsymbol{Y})} \\ &= P(D|S_i, \boldsymbol{Y})P(S_i|\boldsymbol{Y}), \end{aligned} \tag{25}$$

where $P(D|S_i, \boldsymbol{Y})$ is the probability of having a given DMT symbol in state S_i, which happens to be in a set of D successive DMT symbols all being in state S_i. Let us denote the number of states S_i with the duration of D as $k_{S_i,D}$. Then we have $\sum_{D=1}^{\infty} k_{S_i,D} = K_i$ and $p(D|S_i) = \frac{k_{S_i,D}}{K_i}$. We can show that

$$P(D|S_i, \boldsymbol{Y}) = \frac{Dk_{S_i,D}}{\mathcal{E}[D_{S_i,k}]K_i} = \frac{Dp(D|S_i)}{\mathcal{E}[D_{S_i,k}]}. \tag{26}$$

By substituting (29) and (26) into (25), we have

$$\begin{aligned} P(D, S_i|\boldsymbol{Y}) &= \frac{Dp(D|S_i)}{\mathcal{E}[D_{S_i,k}]} \frac{\mathcal{E}[D_{S_i,k}]}{\mathcal{E}[D_{S_0,k}] + \mathcal{E}[D_{S_1,k}]} \\ &= \frac{Dp(D|S_i)}{\mathcal{E}[D_{S_0,k}] + \mathcal{E}[D_{S_1,k}]}. \end{aligned} \tag{27}$$

D. $p(n_I)$ STUDY

Let us now denote the probability of having a received DMT symbol in which the number of samples in state s_1 in the time domain is n_I by $p(n_I)$. According to Appendix D, we then have (28), as shown at the top of the next page. The Cumulative density function (CDF) of n_I at the location of DT central office (CO) and DT customer premises (CP) is shown in Fig. 6.

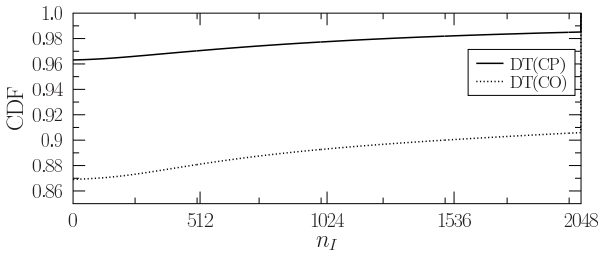

FIGURE 6. Cumulative density function of n_I at DT central offices (CO) and DT customer premises (CP).

V. ANALYSIS OF THE NOISE POWER AND OF THE AVERAGE BIT ERROR RATIO

A. COLOURED NON-GAUSSIAN NOISE IN THE DMT/OFDM SYSTEM

It is widely recognized that the performance of the communication system operating both with or without DMT/OFDM is identical in an AWGN channel. This is because during the DMT/OFDM demodulation the received signals are processed by the DFT-based demodulator, which is a linear process. Hence the linearly processed Gaussian distributed noise also yields a Gaussian distribution with an identical mean and variance after DFT and normalization. The stationary noise is characterized by the above situation. However, the situation is different for the case of the correlated Weibull-distributed impulsive noise in DSL.

$$p(n_I) = \begin{cases} \dfrac{\mathcal{E}[D_{S_0,k}]}{\mathcal{E}[D_{S_0,k}] + \mathcal{E}[D_{S_1,k}]}, & \text{if } n_I = 0 \\ \mathcal{D}_1(n_I, B, v_1, t_1) + \mathcal{D}_1(n_I, 1-B, v_2, t_2), & \text{if } n_I = 1, 2, \cdots, N-1 \\ \mathcal{D}_2(B, v_1, t_1) + \mathcal{D}_2(1-B, v_2, t_2), & \text{if } n_I = N \end{cases} \tag{28}$$

There has been a number of publications discussing the Fourier transforms of both correlated and of non-Gaussian distributed signals [57]–[59]. Here let us denote a correlated Weibull distributed variable by $w[k]$ and its discrete Fourier transformed which of size N by

$$W[i] = \mathrm{DFT}\big[w[k]\big] = \sum_{i=0}^{N} e^{-j\frac{2\pi ik}{N}}. \tag{29}$$

The following convergence has been formally proved in [58]

$$\frac{1}{\sqrt{N}}\Big[\Re\big(W[i]\big), \Im\big(W[i]\big)\Big] \Rightarrow \Big[G[i], G[i]\Big], \tag{30}$$

where $G[i]$ is an independent identically distributed (i.i.d.) normal random variable with zero-mean and variance of $S[i]/2$, while $S[i]$ is the power spectral density associated with the ACF of the process, as stated by the Wiener-Khintchine theorem [60].

After DFT, the impulsive noise at the kth subcarrier has a variance of $\sqrt{N}$ times its spectral density and its distribution tends to the Gaussian distribution. Since the signal and the stationary noise are also amplified by the factor of $\sqrt{N}$ after DMT/OFDM demodulation, the factor $\sqrt{N}$ is eliminated by normalization, when considering the BER vs SNR performance.

B. SNR CALCULATION

Let us denote the power spectral density of the impulsive noise by $S(f)$, which can be calculated from the Fourier Transform (FT) of its ACF $R(t)$ as follows

$$\begin{aligned} S(f) &= \mathcal{F}\big[R(t)\big] \\ &= \frac{\beta}{\beta^2 + 4\pi^2(f+\alpha)^2} + \frac{\beta}{\beta^2 + 4\pi^2(f-\alpha)^2}. \end{aligned} \tag{31}$$

Furthermore, let us denote the impedance in DSL by Z and the power of the impulsive noise at the ith subchannel as $\sigma_{I,i}^2$, which can be calculated as:

$$\begin{aligned} \sigma_{I,i}^2 &= \frac{1}{Z}\int_{i\Delta f}^{(i+1)\Delta f} S(f)\,\mathrm{d}f \\ &= \frac{1}{2\pi Z}\Bigg\{ \tan^{-1}\Big(\frac{2\pi\big[(i+1)\Delta f + \alpha\big]}{\beta}\Big) \\ &\qquad - \tan^{-1}\Big(\frac{2\pi\big[i\Delta f + \alpha\big]}{\beta}\Big) \\ &\qquad + \tan^{-1}\Big(\frac{2\pi\big[(i+1)\Delta f - \alpha\big]}{\beta}\Big) \\ &\qquad - \tan^{-1}\Big(\frac{2\pi\big[i\Delta f - \alpha\big]}{\beta}\Big)\Bigg\}, \end{aligned} \tag{32}$$

where Δf is the multicarrier spacing of DMT.

TABLE 2. Parameter values for different modems.

	BPSK	QPSK	16QAM	64QAM
$[\rho_1, \beta_1]$	$[1, \sqrt{2}]$	$[1, 1]$	$[\frac{3}{4}, \sqrt{\frac{1}{5}}]$	$[\frac{7}{12}, \sqrt{\frac{1}{21}}]$
$[\rho_2, \beta_2]$	\	\	$[\frac{1}{2}, 3\sqrt{\frac{1}{5}}]$	$[\frac{1}{2}, 3\sqrt{\frac{1}{21}}]$
$[\rho_3, \beta_3]$	\	\	$[-\frac{1}{4}, 5\sqrt{\frac{1}{5}}]$	$[-\frac{1}{12}, 5\sqrt{\frac{1}{21}}]$
$[\rho_4, \beta_4]$	\	\	\	$[\frac{1}{12}, 9\sqrt{\frac{1}{21}}]$
$[\rho_5, \beta_5]$	\	\	\	$[-\frac{1}{12}, 13\sqrt{\frac{1}{21}}]$

Since the Fourier transform constitutes a linear process, the Fourier transform of the sum of stationary noise and impulsive noise is equivalent to the sum of Fourier transform of the stationary noise and that of the impulsive noise. Let us introduce $\kappa_i = \frac{\sigma_{I,i}^2}{\sigma_S^2}$ and denote the noise power at the ith subchannel by $\sigma_{N,i}^2$, which can be expressed as [34]

$$\begin{aligned} \sigma_{N,i}^2 &= \frac{N\sigma_S^2 + n_I\sigma_{I,i}^2}{N} \\ &= \Big(1 + \frac{n_I\kappa_i}{N}\Big)\sigma_S^2. \end{aligned} \tag{33}$$

According to (6) and (33), the instantaneous SNR per symbol for the ith subchannel is given by

$$\begin{aligned} \gamma_{i,n_I} &= \frac{|H_i|^2 E_b \cdot M}{(1 + \frac{n_I\kappa_i}{N})\sigma_S^2} \\ &= \frac{|H_i|^2}{1 + \frac{n_I\kappa_i}{N}} \cdot \gamma_{s_0} \cdot M, \end{aligned} \tag{34}$$

where H_i is the gain of the ith subchannel, E_b is the signal power per bit, M is the number of bits per symbol and $\gamma_{s_0} = E_b/\sigma_S^2$. The above equation shows that the SNR of a specific subchannel is affected by its gain, by SNR experienced in the absence of impulsive noise, by the number of samples encountered at state s_1 and by the power ratio between the impulsive noise to stationary noise.

C. BER ANALYSIS

Bearing in mind the convergence of (30), the BER of Q-ary QAM relying on classic Gray mapping for the instantaneous SNR γ_{i,n_I} can be approximated according to the generalized superposition of Q functions [61]:

$$P_e(\gamma_{i,n_I}) \approx \sum_l p_l Q(\beta_l\sqrt{\gamma_{i,n_I}}), \tag{35}$$

where p_l and β_l are different for different modulation schemes, as shown in Table 2. Since the BER in (35) is conditioned on $p(n_I)$, the average BER of the system can be

expressed as

$$P_{b,\mathrm{OFDM}} \approx \frac{1}{N}\sum_{i=0}^{N-1}\sum_{n_I=0}^{N} P_e(\gamma_{i,n_I})p(n_I). \tag{36}$$

Specifically, since the symbols of the subchannels with the index spanning from 1 to $(\frac{N}{2}-1)$ are actually used for demodulation in DMT, the corresponding BER formula of DMT is expressed as

$$P_{b,\mathrm{DMT}} \approx \frac{1}{N/2-1}\sum_{i=1}^{N/2-1}\sum_{n_I=0}^{N} P_e(\gamma_{i,n_I})p(n_I). \tag{37}$$

Substituting (28) and (35) into (37), the average BER of the DMT system under impulsive noise in DSL can be expressed as in (38), as shown at the bottom of this page.

VI. PERFORMANCE EVALUATION

This section first describes on simulation set up, including the DMT, the measured channel and the impulsive noise in conjunction with our modified generation methods. Later, we present our analytical and simulation based BER performance for the DMT-aided DSL for a bandwidth of up to 106 MHz. For the BER performance evaluation, the noise process was arranged to have a sufficiently long duration for ensuring the statistical relevance of the noise model.

A. DMT, CHANNEL AND NOISE

As proposed in G.fast [3], the DMT modulation employs Q-ary QAM on each tone, with the spacing of 51.75 kHz. The DMT symbol rate is 48000 symbol/s, and again the duration T_{DMT} of a DMT symbol is 20.83 μs.

Since there is still no established channel model for the frequency range of G.fast at the time of writing, here we directly utilize the channel measured by BT, which is shown in Fig 7. The low-pass characteristics reflected in the figure are imposed by impedance mismatching, implying that the impedance was designed to be matched at the low frequencies for voice signals, hence the higher frequencies beyond the originally designed frequency range are severely attenuated.

The stationary noise voltage amplitude is modelled by the white Gaussian noise process, with the power spectral density being -135 dBm/Hz. For the impulsive noise, the voltage amplitude and impulse duration is represented by the DT(CP) of Table 1. The inter-arrival time and spectral characteristics

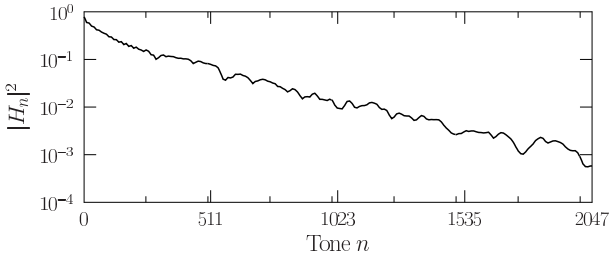

FIGURE 7. The frequency selective channel model in the frequency domain of DSL measured by BT, with a bandwidth of up to 106 MHz and multicarrier spacing of 51.75 kHz. The twisted pairs have a diameter of 0.5 mm and length of 100 m.

are set according to Section II.B. For the LUT generation, we have dropped c_k beyond the ninth in (17), which are indeed negligible.

The desired and simulated power of the impulsive noise is plotted in Fig 8. It can be inferred from the figure that the impulsive noise power has a maximum value at low frequencies, which is about 80 dB higher than the stationary noise floor, and decreases rather sharply, when the frequency becomes higher, in a generated impulsive noise power of about 10 dB higher than the stationary noise floor. Compared to [20, 14], the simulated results seen in Fig 8 demonstrates a substantial improvement: the simulated power is quite close to the analytical one in our proposed method, while there is at least 10 dB gap between the desired and simulated impulsive noise power at the peak values in [20]. However, as the filter employed still fails to perfectly reflect the spectral characteristics of the impulsive noise, without loss of generality, we substitute the simulated impulsive noise power into (38), when calculating the analytical results. This provides us with an accurate semi-analytical result for comparison.

B. BER PERFORMANCE

In Fig 9, we investigate the BER performance of the DMT system considered under non-dispersive channel conditions while inflicting both stationary and impulsive noise in DSL. In this figure, three different modulation schemes, namely 4QAM, 16QAM and 64QAM are considered. In addition to the well-known features of the different classic modulation schemes, our observations are as follows. Firstly, in comparison to the performance experienced over benign AWGN channels, there is a gradual slope change beyond a certain

$$\begin{aligned} P_{b,\mathrm{DMT}} \approx \frac{1}{N/2-1}\sum_{i=1}^{N/2-1}\Bigg\{ & P_e\big(|H_i|^2\gamma_{s_0}\big)\cdot\frac{\mathcal{E}[D_{S_0,k}]}{\mathcal{E}[D_{S_0,k}]+\mathcal{E}[D_{S_1,k}]} \\ & + \sum_{n_I=1}^{N-1} P_e\Big(\frac{|H_i|^2\gamma_{s_0}}{1+\frac{n_I\kappa_i}{N}}\Big)\Big[\mathcal{D}_1(n_I,B,v_1,t_1)+\mathcal{D}_1(n_I,1-B,v_2,t_2)\Big] \\ & + P_e\Big(\frac{|H_i|^2}{1+\kappa_i}\gamma_{s_0}\Big)\Big[\mathcal{D}_2(B,v_1,t_1)+\mathcal{D}_2(1-B,v_2,t_2)\Big]\Bigg\} \end{aligned} \tag{38}$$

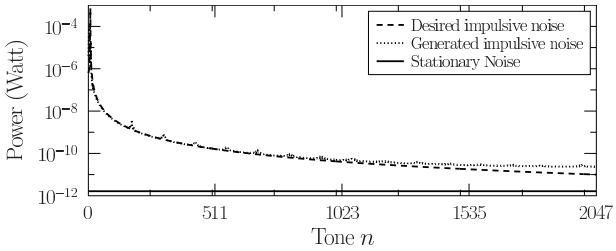

FIGURE 8. Spectrum of the impulsive noise and the stationary noise, with the bandwidth of up to 106 MHz and multicarrier spacing of 51.75 kHz. The desired impulsive noise is plotted according to (32) and the simulated impulsive noise is generated according to the method in Section II.C. For the stationary noise, the power spectral density is set as −135 dBm/Hz.

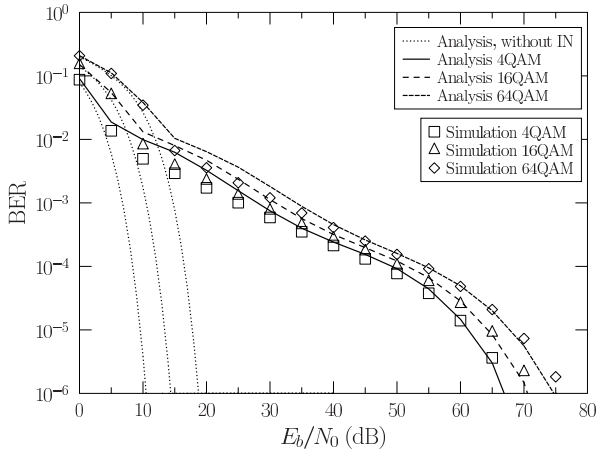

FIGURE 9. BER performance of the DMT system for Q-ary QAM with simulation results and theoretical analysis, when communicating over non-dispersive channels suffering from both stationary and impulsive noise. The theoretical results are calculated according to Eq. (38).

value of γ_{s_0}. This implies that when γ_{s_0} is lower than this value, the BER performance is dominated by the AWGN, while it is more dominated by the impulsive noise, when γ_{s_0} becomes higher. Secondly, in Fig 8, the maximum value of impulsive noise is about 80 dB higher than the stationary noise, while there is a γ_{s_0} gap of 60 dB between the system operating with and without impulsive noise for a given BER of 10^{-6}. The associated performance tends to be higher at higher γ_{s_0} values. This implies that at a high γ_{s_0}, the BER performance of the system is dominated by the maximum value of the impulsive noise.

In Fig 10, we study the BER performance of the DMT system considered, when communicating over dispersive channels using various M-QAM schemes. Firstly, when the channel becomes dispersive, the BER performance is severely degraded at the γ_{s_0} values, where the AWGN dominates the BER performance. In comparison to Fig 9, for a given BER of 10^{-2}, where the AWGN dominates the BER performance, the dispersive channel requires about 20 dB higher γ_{s_0} values, than communicating over non-dispersive channels in order to achieve the same BER performance. This can be explained by the frequency-dependent attenuation shown in Fig 8. It should be noted that although the maximum attenuation is 30 dB in Fig 8, the extra γ_{s_0} required by the

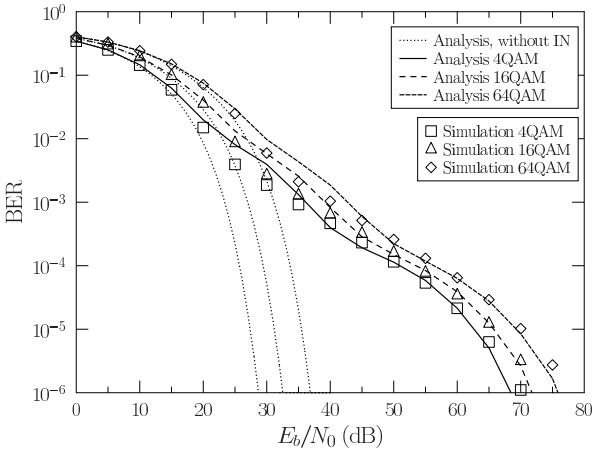

FIGURE 10. BER performance of the DMT system for Q-ary with simulation results and theoretical analysis, QAM when communicating over dispersive channels suffering from both stationary and impulsive noise. The theoretical results are calculated according to Eq. (38).

dispersive channel at BER of 10^{-2} is only about 20 dB. This is explained by the fact that all the tones with the index spanning from 1 to $(\frac{N}{2}-1)$ are utilized in DMT demodulation and the maximum attenuation is 20 dB in the first half of the tones in Fig 7. Secondly, the BER performance at high γ_{s_0} values, where the impulsive noise dominates the performance, is not degraded so severely. For a given BER of 10^{-6}, communicating over dispersive DSL channels requires only 2 dB higher γ_{s_0} than communicating over non-dispersive channels. As previously discussed, the BER performance at high γ_{s_0} values depends on the maximum value of impulsive noise power across the tones. As shown in Fig 8, the first half of the tones associated with the maximum value of the impulsive noise power are at low frequencies, where the channels' attenuation is low as shown in Fig 8, hence only resulting in a modest performance degradation.

In Fig 11, we explore the effect of the receiver location on the BER performance of DMT-based DSL systems contaminated both non-dispersive and dispersive channels, in the presence of both the stationary and the impulsive noise. In this figure, DT's central offices and DT's customer premises are considered. The corresponding impulsive noise characteristics are parametrized according to Table 1. Our observations are listed below. Firstly, for both non-dispersive and dispersive channels, the CO has a smaller γ_{s_0} value, where the impulsive noise dominates the BER performance. In other words, the CPs benefit from a better performance than the CO. As discussed in Section I, the receivers at the CO inevitably suffers from more dialling pulses, busy signals and ringing, which causes longer impulsive noise burst. Quantitatively, the mean value of the impulsive noise duration is 34.87 μs at DT(CP) and 157.22 μs at DT(CO) as calculated from the distribution in (9). According to (38), the probability of a DMT symbol becoming impaired by impulsive noise increases, when the impulse duration becomes longer, while keeping the inter-arrival time the same. Secondly, the γ_{s_0} gap between the CO and the CP becomes smaller upon aiming

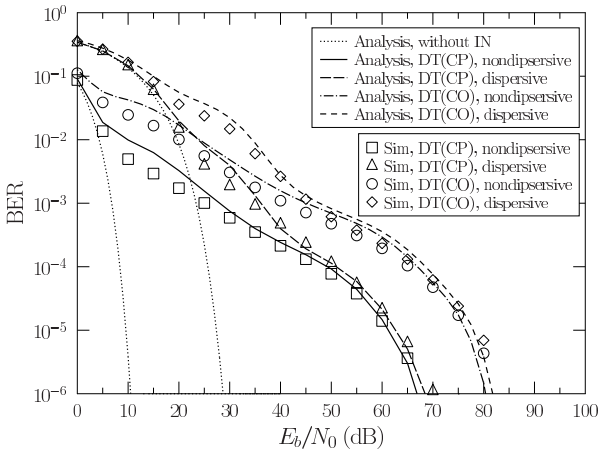

FIGURE 11. BER performance of the DMT system at the Deutsche Telekom central offices and customer premises with simulation results and theoretical analysis, when communicating over both non-dispersive and dispersive channels suffering both from stationary and impulsive noise. 4QAM is employed. The theoretical results are calculated according to Eq. (38).

for achieving the same BER, when the maximum impulsive noise power dominates the BER performance. This can be explained by bearing in mind that at high γ_{s_0} the BER performance is mainly degraded, because the high-power impulsive noise requires a sufficiently high signal power to correct the errors, while at high γ_{s_0} the BER performance mainly depends on $\mathcal{E}[n_I]$ and $\sigma_{I,i}^2$, as seen with the aid of (38).

VII. CONCLUSIONS

In this paper, we have improved the methods in [20] by providing computationally convenient expressions confirmed by our simulation results, which prove that the impulsive noise generated reflects the practical DSL spectral characteristics. We analysed the performance of DMT systems both under practical noise conditions and under dispersive DSL channel conditions with the aid of a hidden semi-Markov model. A closed-form BER formula was derived for DMT-based DSL systems. The simulation results demonstrated the accuracy of the BER formulas and showed that the BER performance of our DMT-based DSL systems is severely degraded both by the impulsive noise and by dispersive channels.

Cognitive radio (CR) capabilities have been exploited in telecommunication networks [62]–[65]. For the future work, we plan to incorporate the CR concept to the multiuser DSL in the presence of impulsive noise, especially from the aspect of physical and data-link layer.

Appendix A
Derivation of $p(d|s_i)$

A. STATE s_0

For a Markov process having a one-step transition probability matrix of

$$\mathbf{P}_{s_0}(1) = \begin{bmatrix} p_{s_0}^{00} & p_{s_0}^{01} \\ p_{s_0}^{10} & p_{s_0}^{11} \end{bmatrix} \tag{39}$$

according to [66], we have

$$\lim_{n\to+\infty} \mathbf{P}_{s_0}^{00}(n) = \lim_{n\to+\infty} \mathbf{P}_{s_0}^{10}(n) = \frac{p_{s_0}^{10}}{p_{s_0}^{01}+p_{s_0}^{10}}, \tag{40}$$

$$\lim_{n\to+\infty} \mathbf{P}_{s_0}^{01}(n) = \lim_{n\to+\infty} \mathbf{P}_{s_0}^{11}(n) = \frac{p_{s_0}^{01}}{p_{s_0}^{01}+p_{s_0}^{10}}. \tag{41}$$

Since the probability matrix is a simple (2×2)-element matrix, the transition probability exhibit rapid convergence. Let us denote $\frac{p_{s_0}^{10}}{p_{s_0}^{01}+p_{s_0}^{10}}$ by $\pi_{0,0}$ and $\frac{p_{s_0}^{01}}{p_{s_0}^{01}+p_{s_0}^{10}}$ by $\pi_{0,1}$. For $d < [t_s/\Delta t]$, the PMF of state s_0 can be expressed as

$$\begin{aligned} p(d|s_0) &= \pi_{0,0} \int_{(d-0.5)\Delta t}^{(d+0.5)\Delta t} f(t|s_{0,0})\,\mathrm{d}t \\ &= \frac{\pi_{0,0}\left(e^{-\lambda\Delta t(d-0.5)} - e^{-\lambda\Delta t(d+0.5)}\right)}{1-e^{-\lambda t_s}}, \end{aligned} \tag{42}$$

and for $d \geq [t_s/\Delta t]$, we have

$$\begin{aligned} p(d|s_0) &= \pi_{0,1} \textstyle\int_{(d-0.5)\Delta t}^{(d+0.5)\Delta t} f(t|s_{0,1})\,\mathrm{d}t \\ &= \pi_{0,1}\left(\tfrac{t_s}{\Delta t}\right)^{\theta}\left(\tfrac{1}{(d-0.5)^{\theta}} - \tfrac{1}{(d+0.5)^{\theta}}\right). \end{aligned} \tag{43}$$

B. STATE s_1

$$\begin{aligned} p(d|s_1) &= \int_{(d-0.5)\Delta t}^{(d+0.5)\Delta t} f(t|s_1)\,\mathrm{d}t \\ &= B\left[Q\left(\frac{\ln(\frac{(d-0.5)\Delta t}{t_1})}{v_1}\right) - Q\left(\frac{\ln(\frac{(d+0.5)\Delta t}{t_1})}{v_1}\right)\right] \\ &\quad + (1-B)\left[Q\left(\frac{\ln(\frac{(d-0.5)\Delta t}{t_2})}{v_2}\right)\right. \\ &\quad \left. - Q\left(\frac{\ln(\frac{(d+0.5)\Delta t}{t_2})}{v_2}\right)\right], \end{aligned} \tag{44}$$

where $Q(\cdot)$ is the tail function of the standard normal distribution.

Appendix B
Derivation of $p(D|S_i)$

C. STATE S_0

As shown in (22), the duration relationship between the state s_0 and the state S_0 is categorized into three cases. Let us denote by $p(D|d, s_i)$ the occurrence probability of a suitable η so that the state s_i with the duration of d results in state S_i with the duration of D, where we have $i \in \{0, 1\}$. When exploiting that d and η are independent variables, we have

$$\begin{aligned} p(D|S_0) &= p(D|d, s_0)p(d|s_0)\big|_{d=DN} \\ &\quad + \sum_{d=DN+1}^{(D+1)N-1} p(D|d, s_0)p(d|s_0) \\ &\quad + \sum_{d=(D+1)N}^{(D+2)N-2} p(D|d, s_0)p(d|s_0) \end{aligned}$$

$$= \frac{1}{N}p(d|s_0)\big|_{d=DN} + \sum_{d=DN+1}^{(D+1)N-1}\frac{d-DN+1}{N}p(d|s_0) + \sum_{d=(D+1)N}^{(D+2)N-2}\frac{(D+2)N-d-1}{N}p(d|s_0), \tag{45}$$

for $D = 1, 2, 3\cdots$.

For $d = (D+2)N - 2 < [t_s/\Delta t]$, i.e. $D < \frac{[t_s/\Delta t]+2}{N} - 2$, substituting (42) into (45), we arrive at

$$p(D|S_0) \approx \frac{\pi_{0,0}}{1-e^{-\lambda t_s}}\frac{1}{\lambda\Delta t}\frac{1}{N}\Big(e^{-DN\lambda\Delta t} - 2e^{-(D+1)N\lambda\Delta t} + e^{-(D+2)N\lambda\Delta t}\Big). \tag{46}$$

For $d = DN \geq [t_s/\Delta t]$, i.e. $D \geq \frac{[t_s/\Delta t]}{N}$, substituting (43) into (45), we have

$$p(D|S_0) = \frac{\pi_{0,1}}{N}\Big(\frac{t_s}{\Delta t}\Big)^{\theta}\frac{N^{1-\theta}}{\theta-1}\Big(D^{1-\theta} - 2(D+1)^{1-\theta} + (D+2)^{1-\theta}\Big). \tag{47}$$

Although the inter-arrival time is modelled by two states, the difference of $p(D|S_0)$ among the threshold values should be negligible. Therefore, it is reasonable to extend (46) to $D < \frac{t_s/\Delta t}{N} - 1$ and (47) to $D \geq \frac{t_s/\Delta t}{N} - 1$. In this case, $\sum_{D=0}^{\infty} p(D|S_0)$ is also extremely close to 1.0, which demonstrates the feasibility of the above approximation.

D. STATE S_1

The calculation of $p(D|S_1)$ is categorized into two types: one of is when is the duration of state s_1 in the time domain is shorter than N and occurs within one DMT symbol. Then, we have

$$\begin{aligned} p(D|S_1) &= \sum_{d=1}^{N} p(D|d, s_1)p(d|s_1) \\ &= \sum_{d=1}^{N}\frac{N-d+1}{N}p(d|s_1) \\ &= \mathcal{A}(B, v_1, t_1) + \mathcal{A}(1-B, v_2, t_2), \end{aligned} \tag{48}$$

for $D = 1$, where $\mathcal{A}(\cdot)$ is expressed in (49), as shown at the bottom of this page. The other is the state s_1 which lasts more than 1 DMT symbols, when we have

$$\begin{aligned} p(D|S_1) &= \sum_{d=(D-1)N+1}^{DN} p(D|d, s_1)p(d|s_1) + \sum_{d=(D-2)N+1}^{(D-1)N} p(D|d, s_1)p(d|s_1) \\ &= \sum_{d=(D-1)N+1}^{DN}\frac{DN-d+1}{N}p(d|s_1) + \sum_{d=(D-2)N+1}^{(D-1)N}\frac{d-(D-2)N-1}{N}p(d|s_1) \\ &= \mathcal{B}(B, v_1, t_1) + \mathcal{B}(1-B, v_2, t_2), \end{aligned} \tag{50}$$

for $D = 2, 3, 4, \cdots$, where $\mathcal{B}(\cdot)$ is expressed in (51), as shown at the bottom of this page.

$$\mathcal{A}(B, v_1, t_1) = B\Big\{Q\Big(\frac{\ln\left(\frac{0.5\Delta t}{t_1}\right)}{v_1}\Big) - \frac{1}{N}Q\Big(\frac{\ln\left(\frac{(N+0.5)\Delta t}{t_1}\right)}{v_1}\Big)\Big\} - \frac{B}{N}\Big\{(N-0.5)Q\Big(\frac{\ln\left(\frac{(N-0.5)\Delta t}{t_1}\right)}{v_1}\Big) - \frac{t_1}{\Delta t}\exp\Big(\frac{v_1^2}{2}\Big)Q\Big(\frac{\ln\left(\frac{(N-0.5)\Delta t}{t_1}\right)}{v_1} - v_1\Big) - 1.5Q\Big(\frac{\ln\left(\frac{1.5\Delta t}{t_1}\right)}{v_1}\Big) + \frac{t_1}{\Delta t}\exp\Big(\frac{v_1^2}{2}\Big)Q\Big(\frac{\ln\left(\frac{1.5\Delta t}{t_1}\right)}{v_1} - v_1\Big)\Big\} \tag{49}$$

$$\mathcal{B}(B, v_1, t_1) = B\Big\{-(D-2)Q\Big(\frac{\ln\left(\frac{(D-2)N\Delta t}{t_1}\right)}{v_1}\Big) + (2D-2)Q\Big(\frac{\ln\left(\frac{(D-1)N\Delta t}{t_1}\right)}{v_1}\Big) - DQ\Big(\frac{\ln\left(\frac{DN\Delta t}{t_1}\right)}{v_1}\Big)\Big\} + \frac{t_1}{\Delta t}\exp\Big(\frac{v_1^2}{2}\Big)\frac{B}{N}\Big\{Q\Big(\frac{\ln\left(\frac{(D-2)N\Delta t}{t_1}\right)}{v_1} - v_1\Big) - 2Q\Big(\frac{\ln\left(\frac{(D-1)N\Delta t}{t_1}\right)}{v_1} - v_1\Big) + Q\Big(\frac{\ln\left(\frac{DN\Delta t}{t_1}\right)}{v_1} - v_1\Big)\Big\} \tag{51}$$

$$\begin{aligned} \mathcal{E}[D_{S_0,k}] &= \sum_{D=0}^{\infty} Dp(D|S_0) = \sum_{D=0}^{t_p} Dp(D|S_0) + \sum_{D=t_q}^{\infty} Dp(D|S_0) \\ &= \frac{\pi_{0,0}}{1-e^{-\lambda t_s}}\frac{1}{\lambda\Delta t}\frac{1}{N}\Big\{e^{-N\lambda\Delta t} - (t_n+1)e^{-(t_p+1)N\lambda\Delta t} + t_p e^{-(t_p+2)N\lambda\Delta t}\Big\} \\ &\quad + \frac{\pi_{0,1}}{N}\frac{N^{1-\theta}}{\theta-1}\Big(\frac{t_s}{\Delta t}\Big)^{\theta}\Big\{(t_q)^{2-\theta} + (1-t_q)(t_q+1)^{1-\theta}\Big\} \end{aligned} \tag{52}$$

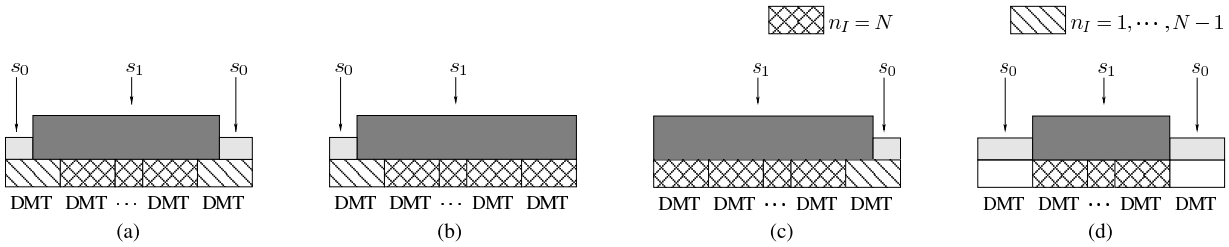

FIGURE 12. Illustration of the locations of $n_I = 1, 2, \cdots, N-1$ and $n_I = N$ in Appendix D.

Appendix C
Expectation of $D_{S_i,k}$

E. STATE 0

When introducing $t_p = \left\lfloor \frac{[t_s/\Delta t]}{N} - 1 \right\rfloor$ and $t_q = \left\lceil \frac{[t_s/\Delta t]}{N} - 1 \right\rceil$, we have (52), as shown at the bottom of the previous page.

F. STATE 1

The expectation of the duration of the state S_1 in the frequency domain can be expressed as

$$\begin{aligned}\mathcal{E}[D_{S_1,k}] &= \sum_{D=0}^{\infty} Dp(D|S_1) \\ &= Dp(D|S_1)\big|_{D=1} + \sum_{D=2}^{\infty} Dp(D|S_1) \\ &= \mathcal{B}(B, v_1, t_1) + \mathcal{B}(1-B, v_2, t_2) \\ &\quad + B \cdot Q\Big(\frac{\ln\left(\frac{N\Delta t}{t_1}\right)}{v_1}\Big) + (1-B)\cdot Q\Big(\frac{\ln\left(\frac{N\Delta t}{t_2}\right)}{v_2}\Big) \\ &\quad + \frac{B}{N}\frac{t_1}{\Delta t}\exp\Big(\frac{v_1^2}{2}\Big)\Big\{2 - Q\Big(\frac{\ln\left(\frac{N\Delta t}{t_1}\right)}{v_1} - v_1\Big)\Big\} \\ &\quad + \frac{1-B}{N}\frac{t_2}{\Delta t}\exp\Big(\frac{v_2^2}{2}\Big)\Big\{2 - Q\Big(\frac{\ln\left(\frac{N\Delta t}{t_2}\right)}{v_2} - v_2\Big)\Big\}. \end{aligned} \tag{53}$$

Appendix D
$p(n_I)$ Study

G. $n_I = 0$

When the number samples in a DMT symbol at state s_1 is 0, we can say that this symbol is in the state S_0. Therefore, we have

$$p(n_I) = P(S_0|\boldsymbol{Y}) = \frac{\mathcal{E}[D_{S_0,k}]}{\mathcal{E}[D_{S_0,k}] + \mathcal{E}[D_{S_1,k}]}, n_I = 0, \tag{54}$$

where $\mathcal{E}[D_{S_0,k}]$ and $\mathcal{E}[D_{S_1,k}]$ can be calculated according to Appendix C.

H. $n_I = 1, 2, \cdots, N-1$

The scenario of $n_I = 1, 2, \cdots, N-1$ is discussed for two specific cases. The first case is when D, namely the number of successive DMT symbols in the state S_1, is larger than 1. In this case, $n_I = 1, 2, \cdots, N-1$ occurs at three locations: 1) as shown in Fig. 12a, the first and the final symbols of the string of symbols in each state S_1 where $D \geq 3$ and the η values are not 0 for the state S_1 and the next state; 2) as shown in Fig. 12b, the first symbol in the each state S_1 where $D \geq 2$ and η value is not 0 for the state S_1 while η value is 0 for the next state; 3) as shown in Fig. 12c, the final symbol in each state S_1 where $D \geq 2$ and η value is 0 for the state S_1 while η value is not 0 for the next state;

$$\begin{aligned}&\Pr_1(1 \leq n_I \leq N-1) \\ &= \sum_{D=3}^{\infty} \frac{2}{D} P(D, S_1|\boldsymbol{Y})\Big(\frac{N-1}{N}\Big)^2 \\ &\quad + \sum_{D=2}^{\infty} \frac{1}{D} P(D, S_1|\boldsymbol{Y}) \frac{1}{N}\frac{N-1}{N} \\ &\quad + \sum_{D=2}^{\infty} \frac{1}{D} P(D, S_1|\boldsymbol{Y}) \frac{1}{N}\frac{N-1}{N}. \end{aligned} \tag{55}$$

In this case, we have $n_I = (N-\eta)$ and η value yields to the uniform distribution. Therefore, the probability of n_I as one of the element in $n_I = 1, 2, \cdots, N-1$ is $(\frac{1}{N-1})$. Consequently, the probability of $n_I = 1, 2, \cdots, N-1$ in this case is given by

$$P_1(n_I) = \frac{1}{N-1}\Pr_1(1 \leq n_I \leq N-1). \tag{56}$$

The second case is $D = 1$ while $1 \leq n_I \leq N-1$. This case can be treated as a state s_1 with the duration $d = n_I$. In order to ensure $D = 1$, the η value has to be within the range $[0, N - n_I + 1]$, with the probability as $(\frac{N-n_I+1}{N})$ for each possible η value. Then, we have

$$P_2(n_I) = \frac{\mathcal{E}[D_{S_1,k}]}{\mathcal{E}[D_{S_0,k}] + \mathcal{E}[D_{S_1,k}]} \frac{N - n_I + 1}{N} p(n_I|s_1). \tag{57}$$

Therefore, the probability of $n_I = 1, 2, \cdots, N-1$ can be expressed as

$$\begin{aligned} P(n_I) &= P_1(n_I) + P_2(n_I) \\ &= \mathcal{D}_1(n_I, B, v_1, t_1) + \mathcal{D}_1(n_I, 1-B, v_2, t_2), \end{aligned} \tag{58}$$

for $n_I = 1, 2, \cdots, N-1$, where $\mathcal{D}_1(\cdot)$ is expressed in (59), as shown at the top of the next page.

I. $n_I = N$

This situation occurs at four locations: 1) as shown in Fig. 12a, the symbols which are not at the first and final symbols in each state S_1 where $D \geq 3$ and the η values are

$$\begin{aligned}\mathcal{D}_1(n_I,B,v_1,t_1) = \frac{N-1}{N^2}\frac{2B}{\mathcal{E}[n_{S_0,k}]+\mathcal{E}[n_{S_1,k}]}\Bigg\{ &-Q\Big(\frac{\ln\left(\frac{N\Delta t}{t_1}\right)}{v_1}\Big)+2Q\Big(\frac{\ln\left(\frac{2N\Delta t}{t_1}\right)}{v_1}\Big)\\ &+\frac{t_1}{\Delta t}\exp\Big(\frac{v_1^2}{2}\Big)\frac{1}{N}\Big[Q\Big(\frac{\ln\left(\frac{N\Delta t}{t_1}\right)}{v_1}-v_1\Big)-Q\Big(\frac{\ln\left(\frac{2N\Delta t}{t_1}\right)}{v_1}-v_1\Big)\Big]\Bigg\}\\ &+\frac{1}{N^2}\frac{2B}{\mathcal{E}[n_{S_0,k}]+\mathcal{E}[n_{S_1,k}]}\Bigg\{Q\Big(\frac{\ln\left(\frac{N\Delta t}{t_1}\right)}{v_1}\Big)+\frac{t_1}{\Delta t}\exp\Big(\frac{v_1^2}{2}\Big)\frac{1}{N}\Big[1-Q\Big(\frac{\ln\left(\frac{N\Delta t}{t_1}\right)}{v_1}-v_1\Big)\Big]\Bigg\}\\ &+\frac{\mathcal{E}[n_{S_1,k}]}{\mathcal{E}[n_{S_0,k}]+\mathcal{E}[n_{S_1,k}]}\frac{N-n_I+1}{N}\Bigg\{B\Big[Q\Big(\frac{\ln(\frac{(n_I-0.5)\Delta t}{t_1})}{v_1}\Big)-Q\Big(\frac{\ln(\frac{(n_I+0.5)\Delta t}{t_1})}{v_1}\Big)\Big]\Bigg\}\end{aligned} \tag{59}$$

$$\begin{aligned}\mathcal{D}_2(B,v_1,t_1) = \frac{(N-1)^2}{N^2}\frac{B}{\mathcal{E}[D_{S_0,k}]+\mathcal{E}[D_{S_1,k}]}\Bigg\{ &-Q\Big(\frac{\ln\left(\frac{N\Delta t}{t_1}\right)}{v_1}\Big)+\frac{1}{N}\frac{t_1}{\Delta t}\exp\Big(\frac{v_1^2}{2}\Big)Q\Big(\frac{\ln\left(\frac{N\Delta t}{t_1}\right)}{v_1}-v_1\Big)\Bigg\}\\ &+\frac{2(N-1)}{N^2}\frac{B}{\mathcal{E}[D_{S_0,k}]+\mathcal{E}[D_{S_1,k}]}\Bigg\{\frac{1}{N}\frac{t_1}{\Delta t}\exp\Big(\frac{v_1^2}{2}\Big)\Bigg\}\\ &+\frac{1}{N^2}\frac{B}{\mathcal{E}[D_{S_0,k}]+\mathcal{E}[D_{S_1,k}]}\Bigg\{Q\Big(\frac{\ln\left(\frac{0.5\Delta t}{t_1}\right)}{v_1}\Big)-\frac{1}{N}Q\Big(\frac{\ln\left(\frac{(N+0.5)\Delta t}{t_1}\right)}{v_1}\Big)\\ &-\frac{1}{N}\Big[(N-0.5)Q\Big(\frac{\ln\left(\frac{(N-0.5)\Delta t}{t_1}\right)}{v_1}\Big)-\frac{t_1}{\Delta t}\exp\Big(\frac{v_1^2}{2}\Big)Q\Big(\frac{\ln\left(\frac{(N-0.5)\Delta t}{t_1}\right)}{v_1}-v_1\Big)\\ &-1.5Q\Big(\frac{\ln\left(\frac{1.5\Delta t}{t_1}\right)}{v_1}\Big)+\frac{t_1}{\Delta t}\exp\Big(\frac{v_1^2}{2}\Big)Q\Big(\frac{\ln\left(\frac{1.5\Delta t}{t_1}\right)}{v_1}-v_1\Big)\Big]\\ &+Q\Big(\frac{\ln\left(\frac{N\Delta t}{t_1}\right)}{v_1}\Big)+\frac{1}{N}\frac{t_1}{\Delta t}\exp\Big(\frac{v_1^2}{2}\Big)\Big[2-Q\Big(\frac{\ln\left(\frac{2N\Delta t}{t_1}\right)}{v_1}-v_1\Big)\Big]\Bigg\}\end{aligned} \tag{60}$$

$$\begin{aligned}P(n_I) &= \sum_{D=3}^{\infty}\frac{D-2}{D}P(D,S_1|\boldsymbol{Y})\frac{N-1}{N}\frac{N-1}{N}+\sum_{D=2}^{\infty}\frac{D-1}{D}P(D,S_1|\boldsymbol{Y})\frac{N-1}{N}\frac{1}{N}\\ &\quad+\sum_{D=2}^{\infty}\frac{D-1}{D}P(D,S_1|\boldsymbol{Y})\frac{1}{N}\frac{N-1}{N}+\sum_{D=1}^{\infty}P(D,S_1|\boldsymbol{Y})\frac{1}{N}\frac{1}{N}\\ &= \frac{(N-1)^2}{N^2}\frac{1}{\mathcal{E}[D_{S_0,k}]+\mathcal{E}[D_{S_1,k}]}\Bigg\{\sum_{D=3}^{\infty}Dp(D|S_1)-2\sum_{D=3}^{\infty}p(D|S_1)\Bigg\}\\ &\quad+\frac{2(N-1)}{N^2}\frac{1}{\mathcal{E}[D_{S_0,k}]+\mathcal{E}[D_{S_1,k}]}\Bigg\{\sum_{D=2}^{\infty}Dp(D|S_1)-\sum_{D=2}^{\infty}p(D|S_1)\Bigg\}\\ &\quad+\frac{1}{N^2}\frac{1}{\mathcal{E}[D_{S_0,k}]+\mathcal{E}[D_{S_1,k}]}\Bigg\{\sum_{D=1}^{\infty}Dp(D|S_1)\Bigg\}\\ &= \mathcal{D}_2(B,v_1,t_1)+\mathcal{D}_2(1-B,v_2,t_2),\\ &\text{for } n_I = N\end{aligned} \tag{61}$$

not 0 for the state S_1 and next state; 2) as shown in Fig. 12b, the symbols which are not the first symbol in each state S_1 where $D \geq 2$ and η value is not 0 for the state S_1 while η value is 0 for the next state; 3) as shown in Fig. 12c, the symbols which are not the final symbol of each state S_1 where $D \geq 2$ and η value is 0 for the state S_1 while η value is not 0 for the next state; 4) as shown in Fig. 12d, all the symbols where $D \geq 1$ and η values are 0 for the state S_1 and the next state. Therefore, $p(n_I)$ can be expressed in (61), as shown at the top of the this page, where $\mathcal{D}_2(\cdot)$ is expressed in (60), as shown at the top of the this page.

REFERENCES

[1] L. Hanzo, S. X. Ng, W. Webb, and T. Keller, *Quadrature Amplitude Modulation: From Basics to Adaptive Trellis-Coded, Turbo-Equalised and Space-Time Coded OFDM, CDMA and MC-CDMA Systems*. Piscataway, NJ, USA: IEEE Press, 2004.

[2] P. Ödling, T. Magesacher, S. Höst, P. O. Börjesson, M. Berg, and E. Areizaga, "The fourth generation broadband concept," *IEEE Commun. Mag.*, vol. 47, no. 1, pp. 62–69, Jan. 2009.

[3] *Fast Access to Subscriber Termials (G. Fast)—Physical Layer Specification*, Doc. ITU-T G.9701, 2014.

[4] M. Timmers, M. Guenach, C. Nuzman, and J. Maes, "G.fast: Evolving the copper access network," *IEEE Commun. Mag.*, vol. 51, no. 8, pp. 74–79, Aug. 2013.

[5] L. Hanzo, M. Münster, B. Choi, and T. Keller, *OFDM and MC-CDMA for Broadband Multi-User Communications, WLANs and Broadcasting*. Hoboken, NJ, USA: Wiley, 2005.

[6] T. Starr, J. M. Cioffi, and P. J. Silverman, *Understanding Digital Subscriber Line Technology*. Englewood Cliffs, NJ, USA: Prentice-Hall, 1999.

[7] W. Yu, G. Ginis, and J. M. Cioffi, "Distributed multiuser power control for digital subscriber lines," *IEEE J. Sel. Areas Commun.*, vol. 20, no. 5, pp. 1105–1115, Jun. 2002.

[8] S. Huberman, C. Leung, and T. Le-Ngoc, "Dynamic spectrum management (DSM) algorithms for multi-user xDSL," *IEEE Commun. Surveys Tuts.*, vol. 14, no. 1, pp. 109–130, 1st Quart., 2012.

[9] G. Ginis and J. M. Cioffi, "Vectored transmission for digital subscriber line systems," *IEEE J. Sel. Areas Commun.*, vol. 20, no. 5, pp. 1085–1104, Jun. 2002.

[10] C. Leung, S. Huberman, K. Ho-Van, and T. Le-Ngoc, "Vectored DSL: Potential, implementation issues and challenges," *IEEE Commun. Surveys Tuts.*, vol. 15, no. 4, pp. 1907–1923, 4th Quart., 2013.

[11] *Very High Speed Digital Subscirber Line (VDSL) Transceivers*, Doc. ITU-T G.993.1, 2005.

[12] W. Henkel and T. Keßler, "A wideband impulsive noise survey in the german telephone network: Statistical description and modeling," *Arch. Elektronik Ubertragungstechnik*, vol. 48, p. 277, Sep. 1994.

[13] S. A. Kassam, *Signal Detection in Non-Gaussian Noise*. Berlin, Germany: Springer, 2012.

[14] M. Ghosh, "Analysis of the effect of impulse noise on multicarrier and single carrier QAM systems," *IEEE Trans. Commun.*, vol. 44, no. 2, pp. 145–147, Feb. 1996.

[15] D. Middleton, "Non-Gaussian noise models in signal processing for telecommunications: New methods an results for class A and class B noise models," *IEEE Trans. Inf. Theory*, vol. 45, no. 4, pp. 1129–1149, May 1999.

[16] J. Nadenau, "Typische störspannungen in fernsprechvermittlungsstellen," in *Proc. NTZ*, vol. 15. 1962, pp. 236–240.

[17] R. M. Fano, "A theory of impulse noise in telephone networks," *IEEE Trans. Commun.*, vol. 25, no. 6, pp. 577–588, Jun. 1977.

[18] W. Henkel, T. Kessler, and H. Y. Chung, "Coded 64-CAP ADSL in an impulse-noise environment-modeling of impulse noise and first simulation results," *IEEE J. Sel. Areas Commun.*, vol. 13, no. 9, pp. 1611–1621, Sep. 1995.

[19] D. B. Levey and S. McLaughlin, "The statistical nature of impulse noise interarrival times in digital subscriber loop systems," *Signal Process.*, vol. 82, no. 3, pp. 329–351, 2002.

[20] I. Mann, S. McLaughlin, W. Henkel, R. Kirkby, and T. Kessler, "Impulse generation with appropriate amplitude, length, inter-arrival, and spectral characteristics," *IEEE J. Sel. Areas Commun.*, vol. 20, no. 5, pp. 901–912, Jun. 2002.

[21] Y. H. Chew, T. T. Tjhung, T. He, and C. C. Ko, "Estimation of BER performance over an impulse noise channel," *Electron. Lett.*, vol. 35, no. 4, pp. 273–274, Feb. 1999.

[22] N. H. Nedev, S. McLaughlin, and D. I. Laurenson, "Estimating errors in transmission systems due to impulse noise," *IEE Proc.–Commun.*, vol. 153, no. 5, pp. 651–656, Oct. 2006.

[23] S. Sugimoto, K. Hayashi, and F. Mano, "Design of 2B1Q transceiver for ISDN subscriber loops," in *Proc. IEEE Int. Conf. Commun. BOSTON-ICC Conf. Rec. World Prosperity Through Commun.*, Jun. 1989, vol. 1, pp. 228–232.

[24] G.-H. Im and J.-J. Werner, "Bandwidth-efficient digital transmission up to 155 Mb/s over unshielded twisted pair wiring," *IEEE J. Sel. Areas Commun.*, vol. 13, no. 12, pp. 1643–1655, Dec. 1995.

[25] B. Daneshrad and H. Samueli, "Performance analysis of a QAM adaptive receiver for 1.6 Mbps digital subscriber line transmission," in *Proc. IEEE Int. Conf. (ICC) Commun. Conf. Rec. SUPERCOMM/ICC Discovering New World Commun.*, Jun. 1992, vol. 2, pp. 937–941.

[26] J. S. Chow, J. C. Tu, and J. M. Cioffi, "A discrete multitone transceiver system for HDSL applications," *IEEE J. Sel. Areas Commun.*, vol. 9, no. 6, pp. 895–908, Aug. 1991.

[27] B. Shim and N. R. Shanbhag, "Complexity analysis of multicarrier and single-carrier systems for very high-speed digital subscriber line," *IEEE Trans. Signal Process.*, vol. 51, no. 1, pp. 282–292, Jan. 2003.

[28] L. Hanzo, T. H. Liew, and B. L. Yeap, *Turbo Coding, Turbo Equalisation and Space-Time Coding*. Hoboken, NJ, USA: Wiley, 2002.

[29] R. G. Gallager, "Low-density parity-check codes," *IRE Trans. Inf. Theory*, vol. 8, no. 1, pp. 21–28, Jan. 1962.

[30] K. J. Kerpez, "Forward error correction for asymmetric digital subscriber lines (ADSL)," in *Proc. Countdown New Millennium Featuring Mini-Theme Pers. Commun. Services Global Telecommun. Conf. GLOBECOM*, Dec. 1991, vol. 3, pp. 1974–1978.

[31] K. J. Kerpez and K. Sistanizadeh, "High bit rate asymmetric digital communications over telephone loops," *IEEE Trans. Commun.*, vol. 43, no. 6, pp. 2038–2049, Jun. 1995.

[32] E. Eleftheriou, S. Olcer, and H. Sadjadpour, "Application of capacity approaching coding techniques to digital subscriber lines," *IEEE Commun. Mag.*, vol. 42, no. 4, pp. 88–94, Apr. 2004.

[33] J. Neckebroek, M. Moeneclaey, M. Guenach, M. Timmers, and J. Maes, "Comparison of error-control schemes for high-rate communication over short DSL loops affected by impulsive noise," in *Proc. IEEE Int. Conf. Commun. (ICC)*, Jun. 2013, pp. 4014–4019.

[34] A. Al-Dweik, A. Hazmi, B. Sharif, and C. Tsimenidis, "Efficient interleaving technique for OFDM system over impulsive noise channels," in *Proc. 21st Annu. IEEE Int. Symp. Pers. Indoor Mobile Radio Commun.*, Sep. 2010, pp. 167–171.

[35] D. Toumpakaris, J. M. Cioffi, and D. Gardan, "Reduced-delay protection of DSL systems against nonstationary disturbances," *IEEE Trans. Commun.*, vol. 52, no. 11, pp. 1927–1938, Nov. 2004.

[36] S. V. Zhidkov, "Analysis and comparison of several simple impulsive noise mitigation schemes for OFDM receivers," *IEEE Trans. Commun.*, vol. 56, no. 1, pp. 5–9, Jan. 2008.

[37] R. Fantacci, A. Tani, and D. Tarchi, "Impulse noise mitigation techniques for xDSL systems in a real environment," *IEEE Trans. Consum. Electron.*, vol. 56, no. 4, pp. 2106–2114, Nov. 2010.

[38] T. Y. Al-Naffouri, A. A. Quadeer, and G. Caire, "Impulse noise estimation and removal for OFDM systems," *IEEE Trans. Commun.*, vol. 62, no. 3, pp. 976–989, Mar. 2014.

[39] H. Zhang, L. L. Yang, and L. Hanzo, "Compressed impairment sensing-assisted and interleaved-double-FFT-aided modulation improves broadband power line communications subjected to asynchronous impulsive noise," *IEEE Access*, vol. 4, pp. 81–96, 2016.

[40] R. Cendrillon, G. Ginis, E. V. D. Bogaert, and M. Moonen, "A near-optimal linear crosstalk canceler for upstream VDSL," *IEEE Trans. Signal Process.*, vol. 54, no. 8, pp. 3136–3146, Aug. 2006.

[41] M. Tomlinson, "New automatic equaliser employing modulo arithmetic," *Electron. Lett.*, vol. 7, no. 5, pp. 138–139, Mar. 1971.

[42] C. B. Peel, B. M. Hochwald, and A. L. Swindlehurst, "A vector-perturbation technique for near-capacity multiantenna multiuser communication—Part I: Channel inversion and regularization," *IEEE Trans. Commun.*, vol. 53, no. 1, pp. 195–202, Jan. 2005.

[43] B. M. Hochwald, C. B. Peel, and A. L. Swindlehurst, "A vector-perturbation technique for near-capacity multiantenna multiuser communication—Part II: Perturbation," *IEEE Trans. Commun.*, vol. 53, no. 3, pp. 537–544, Mar. 2005.

[44] R. Zhang, A. F. Al Rawi, L. D. Humphrey, and L. Hanzo, "Expanded constellation mapping for enhanced far-end-cross-talk cancellation in G.fast," *IEEE Commun. Lett.*, vol. 21, no. 2, pp. 56–59, Jan. 2017.

[45] *Spectrum Management for Loop Transmission Systems*, IEEE Standard T1.417-2001, 2001.

[46] Y. Xu, T. Le-Ngoc, and S. Panigrahi, "Global concave minimization for optimal spectrum balancing in multi-user DSL networks," *IEEE Trans. Signal Process.*, vol. 56, no. 7, pp. 2875–2885, Jul. 2008.

[47] L.-L. Yang, *Multicarrier Communications*. Hoboken, NJ, USA: Wiley, 2009.

[48] S.-Z. Yu, "Hidden semi-Markov models," *Artif. Intell.*, vol. 174, no. 2, pp. 215–243, Feb. 2010.

[49] Y. Ephraim and N. Merhav, "Hidden Markov processes," *IEEE Trans. Inf. Theory*, vol. 48, no. 6, pp. 1518–1569, Jun. 2002.

[50] H. Zhang, L. L. Yang, and L. Hanzo, "Performance analysis of orthogonal frequency division multiplexing systems in dispersive indoor power line channels inflicting asynchronous impulsive noise," *IET Commun.*, vol. 10, no. 5, pp. 453–461, May 2016.

[51] T. Kessler, R. Kirkby, W. Henkel, and S. McLaughlin, "Text for 'realistic impulsive noise model,'" ETSI TM6 011T20, Feb. 2001.

[52] B. Liu and D. Munson, "Generation of a random sequence having a jointly specified marginal distribution and autocovariance," *IEEE Trans. Acoust., Speech, Signal Process.*, vol. 30, no. 6, pp. 973–983, Dec. 1982.

[53] R. Tough and K. Ward, "The correlation properties of Gamma and other non-Gaussian processes generated by memoryless nonlinear transformation," *J. Phys. D, Appl. Phys.*, vol. 32, no. 23, p. 3075, Sep. 1999.

[54] J. C. S. S. Filho and M. D. Yacoub, "Coloring non-Gaussian sequences," *IEEE Trans. Signal Process.*, vol. 56, no. 12, pp. 5817–5822, Dec. 2008.
[55] S. M. Kay and S. L. Marple, "Spectrum analysis—A modern perspective," *Proc. IEEE*, vol. 69, no. 11, pp. 1380–1419, Nov. 1981.
[56] M. Abramowitz and I. A. Stegun, *Handbook of Mathematical Functions: With Formulas, Graphs, and Mathematical Tables*, vol. 55. North Chelmsford, MA, USA: Courier Corporation, 1964.
[57] A. J. Goldsmith and M. Effros, "The capacity region of broadcast channels with intersymbol interference and colored Gaussian noise," *IEEE Trans. Inf. Theory*, vol. 47, no. 1, pp. 219–240, Jan. 2001.
[58] M. Peligrad and W. B. Wu, "Central limit theorem for Fourier transforms of stationary processes," *Ann. Probab.*, vol. 38, no. 5, pp. 2009–2022, Sep. 2010.
[59] E. Bertin and M. Clusel, "Generalized extreme value statistics and sum of correlated variables," *J. Phys. A, Math. General*, vol. 39, no. 24, p. 7607, 2006.
[60] C. Chatfield, *The Analysis of Time Series: An Introduction*. Boca Raton, FL, USA: CRC Press, 2016.
[61] L.-L. Yang and L. Hanzo, "A recursive algorithm for the error probability evaluation of M-QAM," *IEEE Commun. Lett.*, vol. 4, no. 10, pp. 304–306, Oct. 2000.
[62] O. B. Akan, O. B. Karli, and O. Ergul, "Cognitive radio sensor networks," *IEEE Netw.*, vol. 23, no. 4, pp. 34–40, July 2009.
[63] M. Amjad, M. Sharif, M. K. Afzal, and S. W. Kim, "TinyOS-new trends, comparative views, and supported sensing applications: A review," *IEEE Sensors J.*, vol. 16, no. 9, pp. 2865–2889, May 2016.
[64] I. F. Akyildiz, W. Su, Y. Sankarasubramaniam, and E. Cayirci, "A survey on sensor networks," *IEEE Commun. Mag.*, vol. 40, no. 8, pp. 102–114, Aug. 2002.
[65] F. Akhtar, M. H. Rehmani, and M. Reisslein, "White space: Definitional perspectives and their role in exploiting spectrum opportunities," *Telecommun. Policy*, vol. 40, no. 4, pp. 319–331, 2016.
[66] A. Papoulis and S. U. Pillai, *Probability, Random Variables, and Stochastic Processes*. New York, NY, USA: McGraw-Hill, 1985.

TONG BAI (S'15) received the B.Sc. degree in telecommunications from Northwestern Polytechnical University, Xi'an, China, in 2013, and the M.Sc. degree (Hons.) in wireless communications from the University of Southampton, Southampton, U.K., in 2014, where he is currently pursuing the Ph.D. degree with the Southampton Wireless Group. His research interests include copper-based broadband communications and design of communication systems in the presence of impulsive noise.

HONGMING ZHANG (S'15) received the B.Eng. degree (Hons.) in telecommunications jointly from the Nanjing University of Aeronautics and Astronautic and the City University London, in 2011, and the M.Sc. degree in wireless communications from the University of Southampton, Southampton, U.K., in 2012, where he is currently pursuing the Ph.D. degree. His research interests include power line communications, compressed sensing, and the design of communications systems.

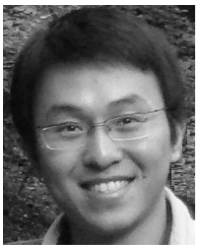

RONG ZHANG (M'09–SM'16) received the Ph.D. degree in wireless communications from the University of Southampton (UoS), Southampton, U.K., in 2009. He was a Research Assistant during that period with the Mobile Virtual Center of Excellence, one of the U.K.'s largest industrial-academic partnerships in ICT. He is currently an Assistant Professor with the Southampton Wireless Group, School of ECS, UoS. He contributed as the UoS Lead Researcher on a number of international projects. He took his industrial consulting leave for Huawei EU Research and Development as a System Algorithms Expert. He has a total of over 80 IEEE/OSA publications, including over 55 journals (over 20 of which he is first author). He was a recipient of the Prestigious Dean's Publication Award. He was also a recipient of the Prestigious RAEng Industrial Fellowship. He regularly serves as a Reviewer of IEEE/OSA journals and funding bodies and has been several times the TPC member/invited session chair of major conferences. He is an RAEng Industrial Fellow and a member of the OSA.

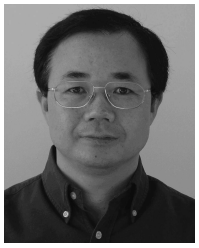

LIE-LIANG YANG (M'98–SM'02–F'15) received the B.Eng. degree in communications engineering from Shanghai TieDao University, Shanghai, China, in 1988, and the M.Eng. and Ph.D. degrees in communications and electronics from Beijing Jiaotong University, Beijing, China, in 1991 and 1997, respectively. In 1997, he was a Visiting Scientist at the Institute of Radio Engineering and Electronics, Academy of Sciences of the Czech Republic. Since 1997, he has been with the University of Southampton, Southampton, U.K., where he is currently a Professor of Wireless Communications with the School of Electronics and Computer Science. His research has covered a wide range of topics in wireless communications, networking, and signal processing. He has authored over 300 research papers in journals and conference proceedings, authored/coauthored three books, and authored several book chapters. He is a Fellow of the IET. He served as an Associate Editor of the IEEE TRANSACTIONS ON VEHICULAR TECHNOLOGY and the *Journal of Communications and Networks*. He is currently an Associate Editor of IEEE ACCESS and the *Security and Communication Networks Journal*.

ANAS F. AL RAWI (S'08–M'13) received the M.Sc. (Hons.) and Ph.D. degrees in communications and signal processing from Newcastle University, U.K., in 2007 and 2011, respectively.

From 2010 to 2012, he was with the School of Electrical and Electronic Engineering, Swansea University, Swansea, U.K., as a Post-Doctoral Researcher. In 2012, he was a Research Associate with the Institute of Electronics, Communications and Information Technology, Queen's University of Belfast, Belfast, U.K. He is currently a Senior Researcher with the Access Network Research Team, Research and Technology, British Telecom, Adastral Park, Martlesham, U.K. His primary role focuses on the modeling of the current wireline technologies and future generations. His research interests include computational electromagnetics, transmission cross-layer optimization, cooperative networks, and multimode MIMO systems modeling.

JIANKANG ZHANG (S'08–M'12) received the B.Sc. degree in mathematics and applied mathematics from the Beijing University of Posts and Telecommunications in 2006, and the Ph.D. degree in communication and information systems from Zhengzhou University in 2012. In 2012, he became a Lecturer with the School of Information Engineering, Zhengzhou University. From 2010 to 2012, he was a Visiting Researcher with Electronics and Computer Science, University of Southampton, Southampton, U.K, where he has been a Research Fellow since 2014. His research interests are in the areas of wireless communications and signal processing, aircraft communication, and wireline communication.

LAJOS HANZO (M'91–SM'92–F'04) received the D.Sc. degree in electronics in 1976 and the Ph.D. degree in 1983. During his 40-year career in telecommunications he has held various research and academic posts in Hungary, Germany, and the U.K. Since 1986, he has been with the School of Electronics and Computer Science, University of Southampton, Southampton, U.K., where he holds the Chair in telecommunications. He has successfully supervised over 100 Ph.D. students, coauthored 18 Wiley/IEEE Press books on mobile radio communications totalling in excess of 10 000 pages, published 1670 research entries on IEEE Xplore, acted both as the TPC and the General Chair of IEEE conferences, presented keynote lectures and been awarded a number of distinctions. He is currently directing a 50-strong academic research team, involved in a range of research projects in the field of wireless multimedia communications sponsored by industry, the Engineering and Physical Sciences Research Council (EPSRC), U.K., the European IST Program, and the Mobile Virtual Center of Excellence, U.K. He is an enthusiastic supporter of industrial and academic liaisons, and he offers a range of industrial courses. He is also a Governor of the IEEE VTS. From 2008 to 2012, he was the Editor-in-Chief of the IEEE Press and a Chaired Professor with Tsinghua University, Beijing. His research is funded by the European Research Council's Senior Research Fellow Grant. He is a Fellow of the IET and EURASIP. In 2009, he was awarded the honorary doctorate *Doctor Honoris Causa* by the Technical University of Budapest and by The University of Edinburgh in 2015.